Simple Electrochemical Detection Methods of Metabolites and Drug with Bare BDD Electrodes

September 2025

ZHANG, Ziping

A Thesis for the Degree of Ph.D. in Science

Simple Electrochemical Detection Methods of Metabolites and Drug with Bare BDD Electrodes

September 2025

Graduate School of Science and Technology
Keio University

ZHANG, Ziping

Table of Contents

Chapter 1 General Introduction

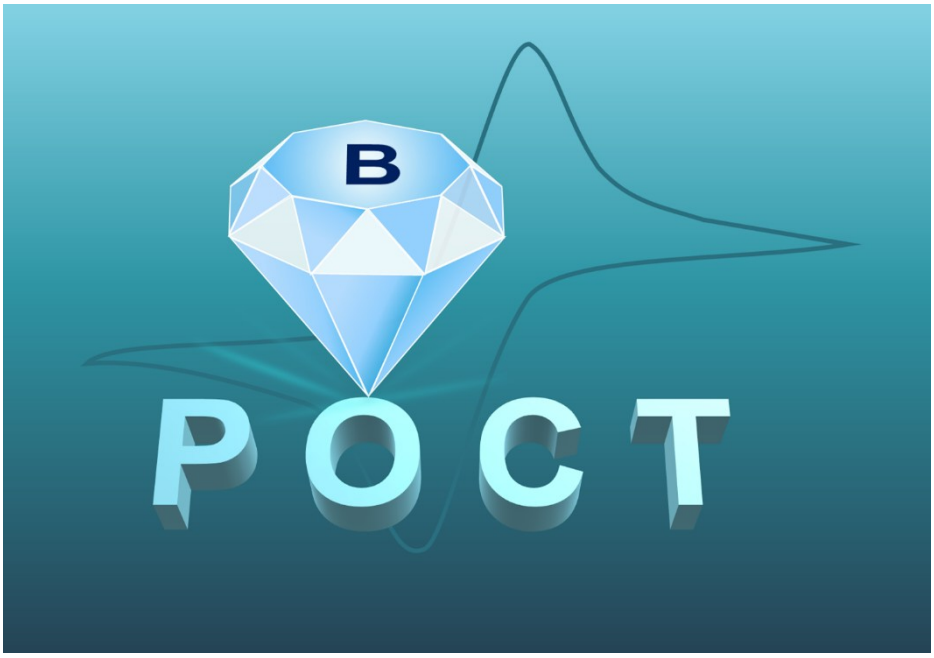

1.1 Point of Care Testing (POCT)

Point-of-care testing (POCT), otherwise referred to as near-patient, bedside, or extra laboratory testing [1]. It can deliver results without having to wait days or even hours for sample transport and laboratory processing [2]. The POCT is affordable, robust and rapid, user-friendly, deliverable, equipment-free [3], high-throughput, in vitro analyses by laypersons [4-6]. It is performed for early instant diagnosis of disease [7], such as urine testing [8], and blood glucose testing [9]. In addition, it also plays a crucial role in environmental monitoring, food safety analysis, and other fields [10] (Scheme 1.1). In some resource-limited settings with the absence of medical infrastructures, lack of trained professionals, and inconveniently rapid result connectivity, POCT becomes essential for instant disease and drug diagnosis, ensuring public health management [3].

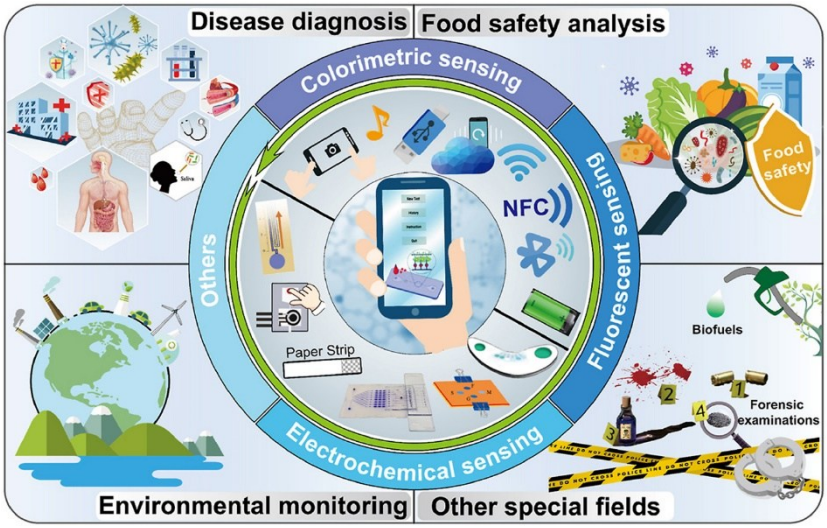

Scheme 1.1 Summary of the application for POCT. Reproduced with permission from TrAC, Trends Anal. Chem. 2022, 157, 116792. Copyright 2022, Elsevier.

1.1.1 Fundamental Design in POCT

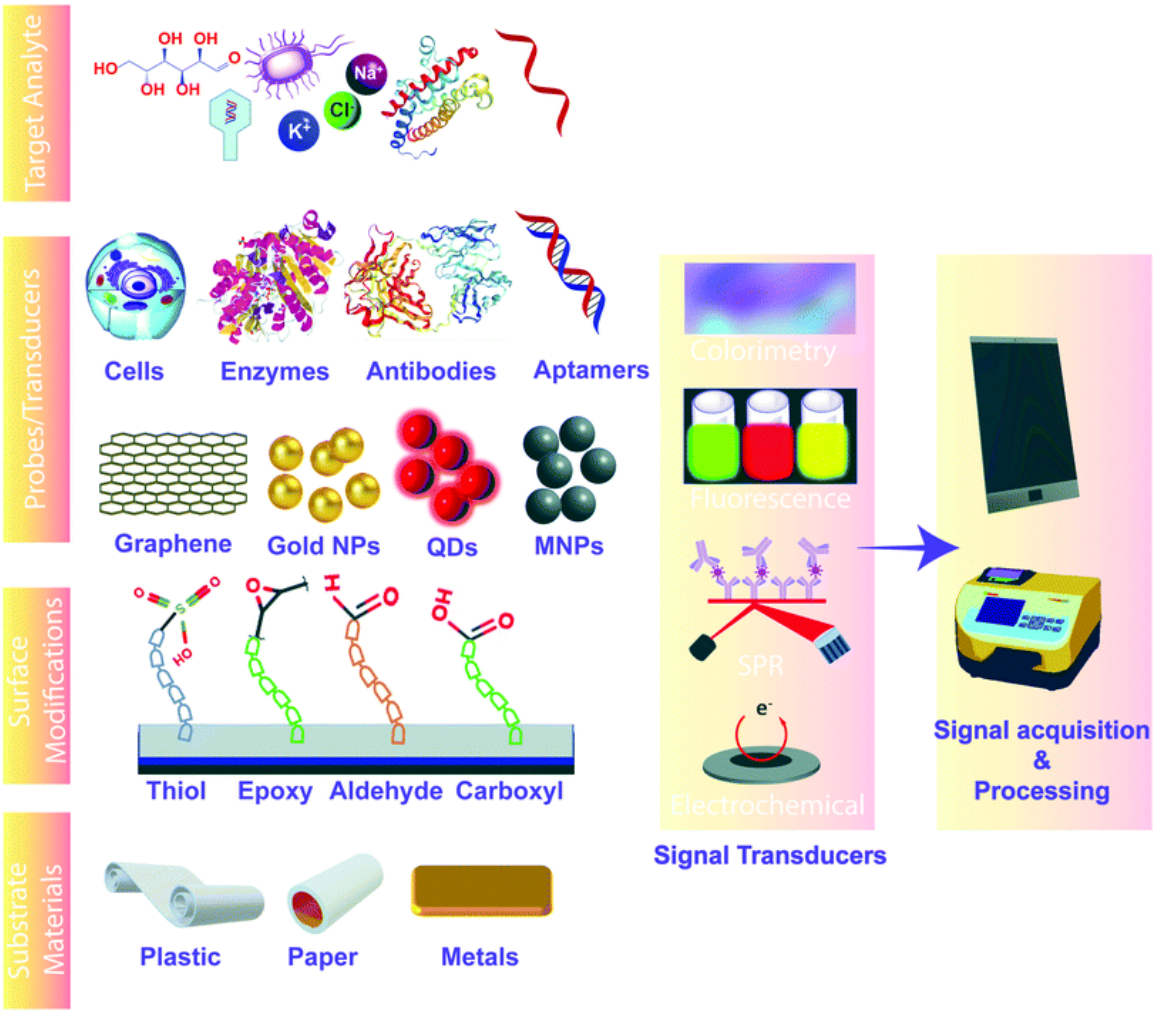

Scheme 1.2 Different components of a fully integrated biosensor including recognition elements, signal transducers, signal acquisition and processing. Reproduced with permission from Chem. Soc. Rev., 2020, 49, 1812 – 1866. Copyright 2020, The Royal of Chemistry.

The Fundamental designs in POCT include several parts: recognition element, signal transducer, platform material, data acquisition, and signal processing (Scheme 1.2). The first step is to choose proper recognition targets. For disease diagnosis and health management in POCT, a variety of recognition elements have been utilized such as protein [11, 12], cell [13], nucleic acid [14-16], drug [4], metabolite [17], or ion [18].

By using different recognition-transduction systems, the POCT

system could convert the chemical reaction into a readable electrical or optical signal, related to the concentration of target analytes. These transducers develop different sensor systems based on different transduction mechanisms, for example, optical sensors, such as using colorimetry, fluorescence, luminescence, and reflectance, or electrochemical sensors with the method of amperometry, voltammetry, and potentiometry.

A variety of materials have been employed to enhance the sensor signals in the interaction between elements and targets. In the biosensing range, metallic nanoparticles, carbon-based materials, magnetic materials, quantum dots, and others have been reported to be used in target analyte detection. Metallic materials, such as Ag or Au nanoparticles have been used in surface-enhanced Raman spectroscopy assay for the specific recognition of bacteria [19] and virus [20]. Carbon-based materials such as graphene, graphene oxide, and carbon nanotubes with large surface area, excellent electrical properties, and catalytic activities, which enhance the sensitivity of detection, have been used in optical and electrochemical sensor [21]. Magnetic particles of iron oxides (γ-Fe_2O_3 and Fe_3O_4) used in biosensors is because of the highly active surface, fast reaction kinetics, high chemical stability, and ease of surface modification [22]. Quantum dots are currently available with various surface modifications, owing to their muti-fold quantum yield and super photostability [23].

Efficient data acquisition and signal processing are important for the results. Optical signals can be read by a digital camera, smartphone camera, or photodetector and analyzed or processed by proper imaging software. The electrochemical sensor is another widely used approach for POCT. The electrical signal of probe-target interactions can be measured by potentiostat and relative software.

1.1.2 Electrochemical Sensors for POCT

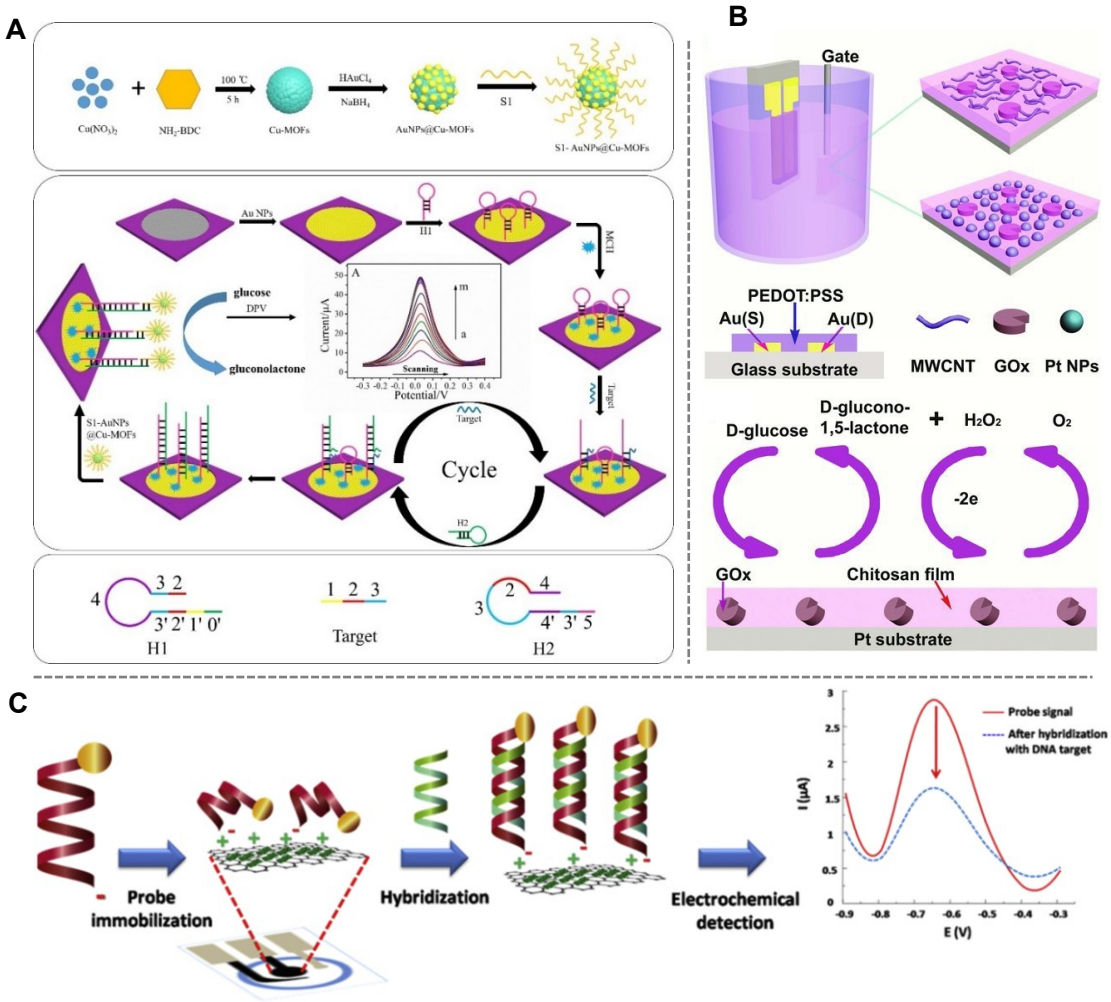

Figure 1.1 Different modified electrodes in biosensing. A, RNA strand-Au nanoparticle @Cu-MOF based electrode for biosensor. Adapted from Sensor Actuat. B Chem., 2018, 257, 561–569. Copyright 2017 Elsevier. **B**, Highly sensitive glucose biosensors based on organic electrochemical transistors using Platinum gate electrodes modified with enzyme and nanomaterials. Adapted from Adv. Funct. Materials, 2011, 21, 2264–2272. Copyright 2011 Wiley-VCH. C, Graphene-polyaniline modified electrode peptide nucleic acid biosensor for detecting human papillomavirus. Adapted from Anal. Chim. Acta., 2017, 952, 32–40. Copyright 2017 Elsevier.

Electrochemical sensors possess significant potential in POCT systems. This is due to their high sensitivity, accuracy, specificity, and low detection limits, which can be miniaturized effectively, cost-efficient,

and easy to operate [24, 25]. In an electrochemical sensor, electrical or electrochemical reactions occur at the interface between the working electrode and the target solution. Electrochemical signal transducers catch the electrical signal generated from the reaction of the recognition element and target analyte [26]. Generally, the monitored signals include measurable current (amperometry), charge accumulation or potential (potentiometry), changed conductive properties of the medium between electrodes (conductometry) [27]. In electrochemical detection, the electrodes work as signal transducers with high sensitivity and operational simplicity. Advances in surface modifications of various materials, such as metallic and carbon nanomaterials [28-30], metal-organic frameworks (MOF) [31], polymer [32, 33], and biological entities (protein [34], enzymes [35], etc.) have been reported in several works and studies. Different biosensors with various material modifications are shown in Figure 1.1. Metallic material, such as Gold, is used because of its advances in steadily immobilizing bio-organic materials (such as RNA), and retaining their bioactivities, which is advanced in better and high sensitivity. In addition, metallic materials can enhance the electron transfer between redox centers and bulk materials [36]. Carbon nanomaterials, such as carbon nanotubes [37], carbon dots [38], carbon nanofibers [39], graphene [40], and graphene oxide [41] have been widely used in electrochemical sensor systems. This is due to their high conductivity, low ohmic resistance, stability, repeatability, and robustness in aqueous solutions [42]. Molecularly imprinted polymers-based sensors exhibit good properties including high selectivity, sensitivity, great reliability, low cost, and mechanical, thermal and chemical stability, in addition to being employed as biological receptors (antigen and antibody) [43].

1.2 Boron-doped Diamond

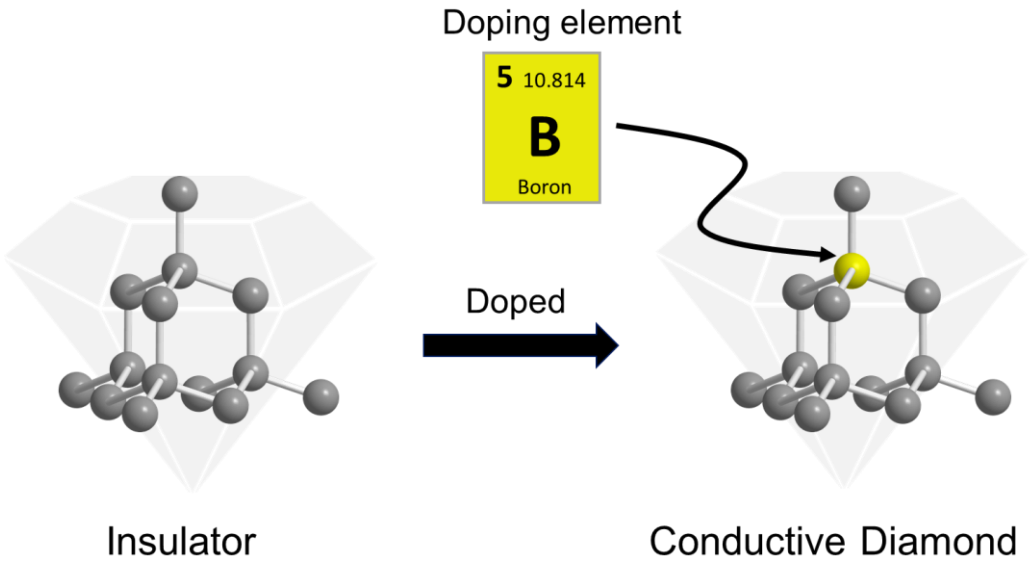

Figure 1.2 Boron-doped diamond.

Intrinsic diamond is seen as a perfect insulator with an ultrawide bandgap of 5.45 eV and extremely high inherent electrical resistivity (10^{16} Ω cm) [44]. Conductive diamond can be obtained by doping impurities, such as nitrogen (N) [45], phosphorus (P) [46] and boron (B) [47]. Boron is easy to incorporate into diamond as a charger acceptor, providing a p-type semiconducting characteristic to diamond. This is due to the boron has one less electron than carbon, and takes up the same position as the displaced carbon atom effectively with an activation energy of 0.37 eV [48, 49] (Figure 1.2). Boron-doped diamond (BDD) is described as semi-metallic or metal-like due to the high doping level enhancing the conductivity and electron-transfer reactivity in the diamond [48].

The highly conducting BDD electrodes have been reported to be widely used in many electrochemical applications, such as drugs [50, 51], biomarkers [52, 53] and heavy metals sensors [54], wastewater treatment [8, 55], ozone generation [56], CO_2 reduction [57], and electrochemical

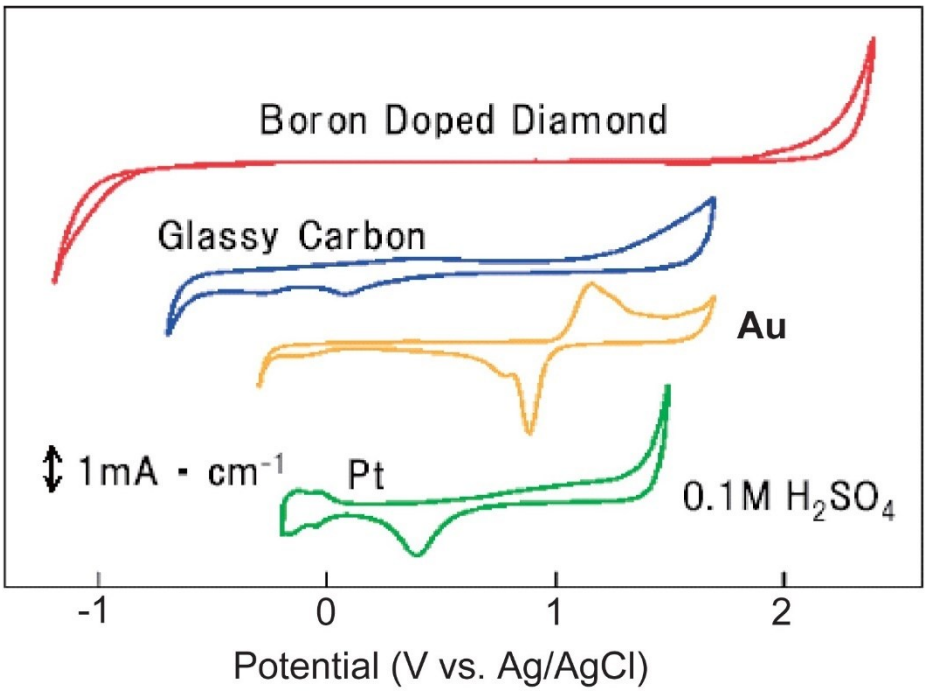

Figure 1.3 Potential windows of various electrodes. Reproduced with permission from Bull. Chem. Soc. Jpn.,2018, 91, 1752–1762. Copyright from Oxford University Press.

organic synthesis [58].

BDD electrodes featured with a wide potential window, can accomplish many important applications that are difficult to achieve by conventional electrodes [44]. Figure 1.3 exhibits the potential windows of various electrodes. Except for the wide potential window, it also could be found from Figure 1.3 that BDD electrodes also have lower background currents. This is attributed to the low capacitance [48], leading to an enhanced signal-to-noise ratio [44]. In addition, BDD electrodes exhibit high stability, biocompatibility, and good resistance to nonspecific absorption [50]. These properties make it possible for detection in complex matrix.

1.3 Outline of the Thesis

This thesis uses the simple electrochemical redox method to measure

metabolites and drugs in human biofluids for sustainable biosensing techniques.

In Chapter 2, the study of urinary $NaNO_2$ selective determination on a bare BDD electrode is described. Without adding other reagents for measurement, such as enzymes, the measurement uses a simple electrochemical approach with an oxidation step followed by reduction. This work focuses on the reduction potential range for the detection. It is different from many previous literature reports on the oxidation reaction. Spiked $NaNO_2$ was determined by cyclic voltammetry and differential pulse voltammetry within two pooled and three individual urine samples. We found that the linear response ranges for sodium nitrite detection were 0.5−10 mg/L (7.2−140 μM) and 10−400 mg/L (140−5800 μM) and obtained the calibration curve, with the LOD being clinically relevant.

In Chapter 3, the selective detection of urinary creatinine (CRE) on a bare BDD electrode is discussed. A similar strategy of electrochemical oxidation followed by reduction is employed. This measurement consists of continuous electrochemical redox of CRE with added reagents of Cl^- and $NaNO_2$. Concentration dependence of CRE in the range of 100−2500 mg/L (0.88–22 mM) and 5−25 mg/L (0.044–0.22 mM) are fulfilled successfully. We tested CRE measurements in two pooled urine and six individual urine samples diluted with D-PBS and 30 mg/L $NaNO_2$. The calculated CRE results have good agreement with those obtained from the Jaffé method. This strategy may potentially detect urinary creatinine, which might be clinically valuable.

In Chapter 4, the edoxaban (EDX) determination on a bare BDD electrode is investigated. In this method, no other reagents are added. EDX is detected by using a similar oxidation followed by a reduction strategy. The study discusses the different electrochemical redox states of EDX on the BDD electrode. The reduction peak for the determination of

EDX can be observed only after the electrochemical oxidation process. In phosphate-buffered saline (PBS), EDX shows a good linearity with the LOD smaller than other electrodes. The same procedure measures EDX in human plasma, and the concentration dependence indicates this method has the feasibility of EDX determination on bare BDD.

1.4 Reference

[1] Price, C. P. Point of care testing. *BMJ* **2001**, 322, 1285-1288.

[2] Drain, P. K.; Hyle, E. P.; Noubary, F.; et al. Diagnostic point-of-care tests in resource-limited settings. *Lancet Infect. Dis.* **2014**, 14, 239-249.

[3] Macovei, D. G.; Irimes, M. B.; Hosu, O.; et al. Point-of-care electrochemical testing of biomarkers involved in inflammatory and inflammatory-associated medical conditions. *Anal. Bioanal. Chem.* **2023**, 415, 1033-1063.

[4] Meng, J.; Tang, X.; Zhou, B.; et al. Designing of ordered two-dimensional gold nanoparticles film for cocaine detection in human urine using surface-enhanced Raman spectroscopy. *Talanta* **2017**, 164, 693-699.

[5] Hang, Y.; Boryczka, J.; Wu, N. Visible-light and near-infrared fluorescence and surface-enhanced Raman scattering point-of-care sensing and bio-imaging: A review. *Chem. Soc. Rev.* **2022**, 51, 329-375.

[6] Song, Y.; Lin, B.; Tian, T.; et al. Recent progress in microfluidics-based biosensing. *Anal. Chem.* **2019**, 91, 388-404.

[7] Zhang, T.; Deng, R.; Wang, Y.; et al. A paper-based assay for the colorimetric detection of SARS-CoV-2 variants at single-nucleotide resolution. *Nat. Biomed. Eng.* **2022**, 6, 957-967.

[8] Tzianni, E. I.; Moutsios, I.; Moschovas, D.; et al. Smartphone paired SIM card-type integrated creatinine biosensor. *Biosens. Bioelectron.* **2022**,

207, 114204.

[9] Haider A.J. Al Lawati; Hassanzadeh, J. Dual-function 2D cobalt metal-organic framework embedded on paper as a point-of-care diagnostic device: Application for the quantification of glucose. *Anal. Chim. Acta* **2020**, 1139, 15-26.

[10] Xing, G.; Ai, J.; Wang, N.; et al. Recent progress of smartphone-assisted microfluidic sensors for point of care testing. *TrAC. Trend. Anal. Chem.* **2022**, 157, 116792.

[11] Puiu, M.; Bala, C. Peptide-based biosensors: From self-assembled interfaces to molecular probes in electrochemical assays. *Bioelectrochemistry* **2018**, 120, 66-75.

[12] Kost, G. J.; Tran, N. K. Point-of-care testing and cardiac biomarkers: The standard of care and vision for chest pain centers. *Cardiol. Clin.* **2005**, 23, 467-490.

[13] Gupta, N.; Renugopalakrishnan, V.; Liepmann, D.; et al. Cell-based biosensors: Recent trends, challenges and future perspectives. *Biosens. Bioelectron.* **2019**, 141, 111435.

[14] Zhang, Y.; Chen, B.; Chen, D.; et al. Electrical detection assay based on programmable nucleic acid probe for efficient single-nucleotide polymorphism identification. *ACS Sensors* **2023**, 8, 2096-2104.

[15] Chen, D.; Huang, W.; Zhang, Y.; et al. CRISPR-mediated profiling of viral RNA at single-nucleotide resolution. *Angew. Chem. Int. Ed.* **2023**, 62, e202304298.

[16] Rezaei, M.; Razavi Bazaz, S.; Zhand, S.; et al. Point of care diagnostics in the age of COVID-19. *Diagnostics* **2020**, 11, 9.

[17] Elusiyan, J. B.; Adeodu, O. O.; Adejuyigbe, E. A. Evaluating the validity of a bedside method of detecting hypoglycemia in children. *Pediatr. Emerg. Care* **2006**, 22, 488-490.

[18] Long, F.; Zhu, A.; Shi, H.; et al. Rapid on-site/in-situ detection of

heavy metal ions in environmental water using a structure-switching DNA optical biosensor. *Sci. Rep.* **2013**, 3, 2308.

[19] Liu, Y. Q.; Zhu, W.; Yuan, Q.; et al. Photoreduced Ag^{+} surrounding single poly(4-cyanostyrene) nanoparticles for undifferentiated SERS sensing and killing of bacteria. *Talanta* **2022**, 245, 123450.

[20] Kaminska, A.; Witkowska, E.; Winkler, K.; et al. Detection of Hepatitis B virus antigen from human blood: SERS immunoassay in a microfluidic system. *Biosens. Bioelectron.* **2015**, 66, 461-467.

[21] Cardenas-Benitez, B.; Djordjevic, I.; Hosseini, S.; et al. Review-covalent functionalization of carbon nanomaterials for biosensor applications: An update. *J. Electrochem. Soc.* **2018**, 165, B103.

[22] Nabaei, V.; Chandrawati, R.; Heidari, H. Magnetic biosensors: Modelling and simulation. *Biosens. Bioelectron.* **2018**, 103, 69-86.

[23] Martynenko, I. V.; Litvin, A. P.; Purcell-Milton, F.; et al. Application of semiconductor quantum dots in bioimaging and biosensing. *J. Mater. Chem. B* **2017**, 5, 6701-6727.

[24] Silva, E. T. S. G. d.; Souto, D. E. P.; Barragan, J. T. C.; et al. Electrochemical biosensors in point-of-care devices: Recent advances and future trends. *ChemElectroChem* **2017**, 4, 778-794.

[25] Dai, Y.; Liu, C. C. Recent advances on electrochemical biosensing strategies toward universal point-of-care systems. *Angew. Chem. Int. Ed.* **2019**, 58, 12355-12368.

[26] Kim, J.; Jeong, J.; Ko, S. H. Electrochemical biosensors for point-of-care testing. *Bio-Design and Manufacturing* **2024**, 7, 548-565.

[27] Grieshaber, D.; MacKenzie, R.; Voros, J.; et al. Electrochemical biosensors-sensor principles and architectures. *Sensors* **2008**, 8, 1400-1458.

[28] Boonkaew, S.; Chaiyo, S.; Jampasa, S.; et al. An origami paper-based electrochemical immunoassay for the C-reactive protein using a

screen-printed carbon electrode modified with graphene and gold nanoparticles. *Mikrochim. Acta* **2019**, 186, 153.

[29] Simioni, N. B.; Silva, T. A.; Oliveira, G. G.; et al. A nanodiamond-based electrochemical sensor for the determination of pyrazinamide antibiotic. *Sens. Actuat. B Chem.* **2017**, 250, 315-323.

[30] El-Wekil, M. M.; Mahmoud, A. M.; Alkahtani, S. A.; et al. A facile synthesis of 3D $NiFe_2O_4$ nanospheres anchored on a novel ionic liquid modified reduced graphene oxide for electrochemical sensing of ledipasvir: Application to human pharmacokinetic study. *Biosens. Bioelectron.* **2018**, 109, 164-170.

[31] Wang, H.; Jian, Y.; Kong, Q.; et al. Ultrasensitive electrochemical paper-based biosensor for microRNA via strand displacement reaction and metal-organic frameworks. *Sens. Actuat. B Chem.* **2018**, 257, 561-569.

[32] Teengam, P.; Siangproh, W.; Tuantranont, A.; et al. Electrochemical paper-based peptide nucleic acid biosensor for detecting human papillomavirus. *Anal. Chim. Acta* **2017**, 952, 32-40.

[33] Ruecha, N.; Shin, K.; Chailapakul, O.; et al. Label-free paper-based electrochemical impedance immunosensor for human interferon gamma detection. *Sens. Actuat. B Chem.* **2019**, 279, 298-304.

[34] Lisdat, F.; Dronov, R.; Möhwald, H.; et al. Self-assembly of electro-active protein architectures on electrodes for the construction of biomimetic signal chains. *Chem. Commun.* **2009**, 274-283.

[35] Ludwig, R.; Ortiz, R.; Schulz, C.; et al. Cellobiose dehydrogenase modified electrodes: Advances by materials science and biochemical engineering. *Anal. Bioanal. Chem.* **2013**, 405, 3637-3658.

[36] Abdulbari, H. A.; Basheer, E. A. M. Electrochemical biosensors: Electrode development, materials, design, and fabrication. *ChemBioEng Rev.* **2017**, 4, 92-105.

[37] Wang, J. Carbon-nanotube based electrochemical biosensors: A review. *Electroanalysis* **2005**, 17, 7-14.

[38] Zhu, X.; Wu, G.; Lu, N.; et al. A miniaturized electrochemical toxicity biosensor based on graphene oxide quantum dots/carboxylated carbon nanotubes for assessment of priority pollutants. *J. Hazard. Mater.* **2017**, 324, 272-280.

[39] Sadrabadi, E. A.; Benvidi, A.; Azimzadeh, M.; et al. Novel electrochemical biosensor for breast cancer detection, based on a nanocomposite of carbon nanofiber, metal-organic framework, and magnetic graphene oxide. *Bioelectrochemistry* **2024**, 155, 108558.

[40] Sethi, J.; Van Bulck, M.; Suhail, A.; et al. A label-free biosensor based on graphene and reduced graphene oxide dual-layer for electrochemical determination of beta-amyloid biomarkers. *Mikrochim. Acta* **2020**, 187, 288.

[41] Wang, Y.; Sauriat-Dorizon, H.; Korri-Youssoufi, H. Direct electrochemical DNA biosensor based on reduced graphene oxide and metalloporphyrin nanocomposite. *Sens. Actuat. B Chem.* **2017**, 251, 40-48.

[42] Ehtesabi, H.; Kalji, S.-O. Carbon nanomaterials for sweat-based sensors: A review. *Mikrochim. Acta* **2024**, 191, 77.

[43] Beluomini, M. A.; da Silva, J. L.; de Sá, A. C.; et al. Electrochemical sensors based on molecularly imprinted polymer on nanostructured carbon materials: A review. *J. Electroanal. Chem.* **2019**, 840, 343-366.

[44] Luong, J. H.; Male, K. B.; Glennon, J. D. Boron-doped diamond electrode: Synthesis, characterization, functionalization and analytical applications. *Analyst* **2009**, 134, 1965-1979.

[45] Zaitsev, A. M.; Kazuchits, N. M.; Kazuchits, V. N.; et al. Nitrogen-doped CVD diamond: Nitrogen concentration, color and internal stress. *Diam. Relat. Mater.* **2020**, 105, 107794.

[46] Katamune, Y.; Izumi, A.; Ichikawa, K.; et al. Heavy phosphorus doping of diamond by hot-filament chemical vapor deposition. *Diam. Relat. Mater.* **2023**, 134, 109789.

[47] Zhen Peng; Jing Xu; Kaori Kurihara; et al. Electrochemical CO_2 reduction on sub-microcrystalline boron-doped diamond electrodes. *Diam. Relat. Mater.* **2021**, 120, 108608.

[48] Muzyka, K.; Sun, J.; Fereja, T. H.; et al. Boron-doped diamond: Current progress and challenges in view of electroanalytical applications. *Anal. Methods* **2019**, 11, 397-414.

[49] Macpherson, J. V. A practical guide to using boron doped diamond in electrochemical research. *Phys. Chem. Chem. Phys.* **2015**, 17, 2935-2949.

[50] Ogata, G.; Ishii, Y.; Asai, K.; et al. A microsensing system for the in vivo real-time detection of local drug kinetics. *Nat. Biomed. Eng.* **2017**, 1, 654-666.

[51] Moriyama, H.; Ogata, G.; Nashimoto, H.; et al. A rapid and simple electrochemical detection of the free drug concentration in human serum using boron-doped diamond electrodes. *Analyst* **2022**, 147, 4442-4449.

[52] He, Y. P.; Lin, H. B.; Guo, Z. C.; et al. Recent developments and advances in boron-doped diamond electrodes for electrochemical oxidation of organic pollutants. *Sep. Purif. Technol.* **2019**, 212, 802-821.

[53] Yu, R.; Deng, Z.; Sharel, P. E.; et al. Highly specific and sensitive quantification of uric acid in sweat using a dual boron-doped diamond electrode. *Sens. Actuat. B Chem.* **2025**, 426, 137031.

[54] Agustiany, T.; Khalil, M.; Einaga, Y.; et al. Stable iridium-modified boron-doped diamond electrode for the application in electrochemical detection of arsenic (III). *Mater. Chem. Phys.* **2020**, 244, 122723.

[55] Natsui, K.; Hosomi, T.; Ikemiya, N.; et al. Electrochemical mineralization of dimethyl sulfoxide on boron-doped diamond electrodes. *Environ. Technol. Innov.* **2019**, 15, 100409.

[56] Honda, Y.; Ivandini, T. A.; Watanabe, T.; et al. An electrolyte-free system for ozone generation using heavily boron-doped diamond electrodes. *Diam. Relat. Mater.* **2013**, 40, 7-11.

[57] Xu, J.; Natsui, K.; Naoi, S.; et al. Effect of doping level on the electrochemical reduction of CO_2 on boron-doped diamond electrodes. *Diam. Relat. Mater.* **2018**, 86, 167-172.

[58] Ikemiya, N.; Natsui, K.; Nakata, K.; et al. Long-term continuous conversion of CO_2 to formic acid using boron-doped diamond electrodes. *ACS Sustain. Chem. Eng.* **2018**, 6, 8108-8112.

Chapter 2 Electrochemical Diagnosis of Urinary Tract Infection Using a Bare BDD Electrode

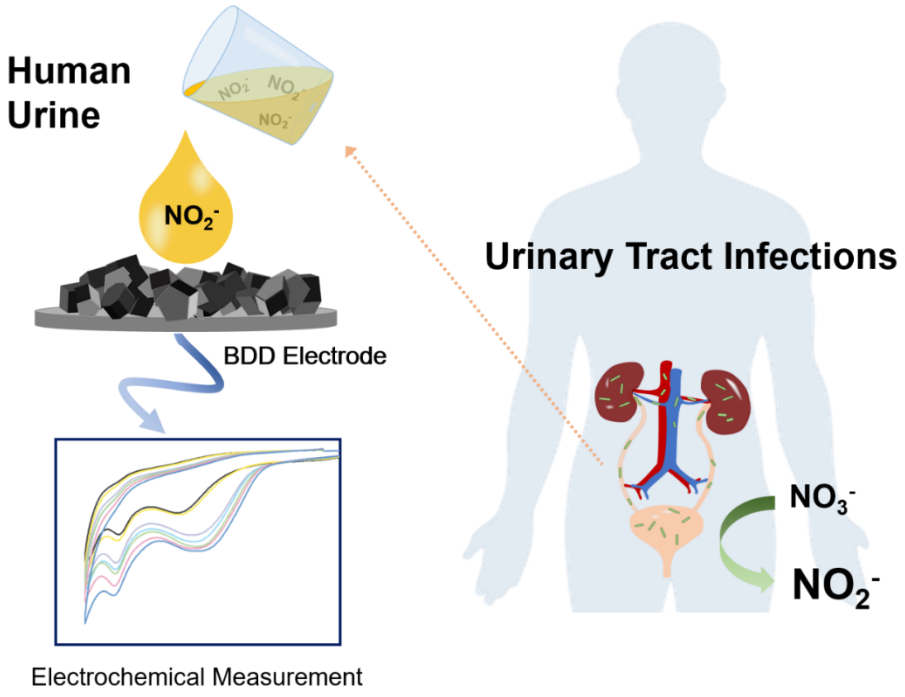

Reproduced with permission from ZP. Zhang, G. Ogata, K. Asai, T. Yamamoto, Y. Einaga, Electrochemical Diagnosis of Urinary Tract Infection Using Boron-Doped Diamond Electrodes. ACS Sens. 2023, 8, 4245 – 4252. Copyright 2023, American Chemical Society

2.1 Introduction

Urinary tract infection (UTI) is one of the most common bacterial infections in the human urinary system. It requires antibiotics and may even result in hospitalization [1]. Due to the frequency and recurrence of UTIs and the global increase in antibiotic resistance, effective diagnosis and treatment of UTIs are essential. However, the existing methods pose significant challenges.

Urine culture is a valuable tool for diagnosing UTIs and can be considered the gold standard method for diagnosis [2, 3]. However, obtaining results of urine culture can take several days, which may delay treatment and increase the risk of complications [4]. Patients' present symptoms, fast nitrite stripe test results, and white blood cell counts in urine are widely employed to diagnose UTIs regularly in hospitals and clinics. However, these methods are time-consuming and require specific conditions, leading to inconvenience in terms of self-diagnosis and self-monitoring.

On the other hand, the presence of nitrites in the urine is a strong indication of UTIs. A dipstick test for sodium nitrite ($NaNO_2$) is an affordable, available, and rapid way to observe UTIs by ourselves [5]. However, a low predictive accuracy [6], a low rate of truly positive results [7], and unclear color recognition can significantly affect frequent UTI self-diagnosis and may lead to incorrect medication guidance and health monitoring. Also, various techniques have been widely adopted in nitrite detection, such as spectrophotometry [8, 9], chemiluminescence [10], chromatography [11, 12], capillary electrophoresis [13, 14], and spectrofluorimetric [15]. However, these analytical techniques for $NaNO_2$ detection are complex, time-consuming, and costly [16-18]. Moreover, careful sample preparation and detailed statistical analysis are important

for accurate results, which require professional training and specific equipment.

Electrochemical methods are more attractive because of their simplicity, sensitivity, rapidity, and low cost [19-21]. However, conventional electrodes such as platinum (Pt), glassy carbon (GC), and carbon paste electrodes (CPE) have rarely been used to directly detect $NaNO_2$ concentrations in human urine due to limitations, such as a narrow potential window, a large background current, and susceptibility to corrosion. These shortcomings are likely to decrease the accuracy and sensitivity of electroanalysis [17]. To address this dilemma, a variety of materials for electrode modification has been introduced to improve the current response signal and extend the potential ranges [22-26]. Nevertheless, the modification of electrodes requires a substantial investment of time and financial resources.

Currently, most nitrite electrochemical detection studies are focused on the oxidation of $NaNO_2$ on surface-modified electrodes. The determination of urinary $NaNO_2$ has rarely been studied directly using a bare electrode due to the limitations of these electrodes, such as a narrow potential window, large overpotential, and easy corrosion. However, because the components of human urine are very complex, with nearly three thousand compounds [27], these complicated biological matrices can be oxidized and generate distinct electrochemical responses (Figure 2.6). Furthermore, the composition and concentration of urine vary from person to person, which would be affected by conditions such as gender, age, drinking, and eating habits [28]. Even the urine of the same person would be affected by normal changes in bodily function. As a result, the background currents of the urine samples are likely to show significant differences from each other. These greatly hinder the application of electrochemical detection of $NaNO_2$ in human urine samples.

2.2 Experimental

2.2.1 Chemicals and Materials

Diamond powder (~1 μm) was obtained from Kemet Japan Co., Ltd. (Japan). Trimethyl borate (TMB) was from Tokyo Chemical Industry Co., Ltd. (Japan). Acetone was supplied by Kanto Chemical Co., Inc. (Japan). Dulbecco's phosphate buffered saline (D-PBS), H_2SO_4 (0.1 M), KCl, $Na_2HPO_4 \cdot 12H_2O$, $NaH_2PO_4 \cdot 2H_2O$, $NaNO_2$, creatinine, ascorbic acid, urea, glucose, uric acid, and agar were purchased from Wako Pure Chemical Industries, Ltd. (Japan). All of the reagents were used without further purification. All of the aqueous solutions were prepared with phosphate buffer (PB), D-PBS (using HCl change pH to 6.4) and deionized water (with a resistivity of 18.2 MΩ cm at 25 °C), which was obtained from DIRECT-Q3 UV (Merck Millipore Corporation, Germany). Urine samples were purchased from Lee BioSolutions, Inc. (USA), and stored at −30 °C. The pH of urine samples was detected by a water quality meter (LAQUA, F-74, HORIBA Advanced Techno, Co., Ltd., Japan), and the details are shown in Table 2.1. Before use, these urine samples were thawed to room temperature (25 °C), disposable filter units (Thermo Fisher Scientific Inc., USA) with polyether sulfone microporous membrane (pore size: 0.45 μm) were used to remove precipitated protein and bacteria. The stock $NaNO_2$ solution (0.5, 1, 2.5, 5, 10, 50, 100, 200, 300, 400 g/L) was frozen at −30 °C until use. Before electrochemistry measurements, they were thawed to room temperature, and 1 μL stock solution was added into 1 mL PB, D-PBS or human urine. In comparison with other electrodes, the 0.05 μm alumina polishing suspension and polishing cloth (PSA backed, 2.875 in) for polishing the GC and Pt electrodes were obtained from Baikowski International Corp. (France) and Buehler Ltd. (USA), respectively.

Table 2.1 The information of human urine.

Urine Samples	Donors	pH
pooled urine 1 (PU1)	≥ 3	6.610
pooled urine 2 (PU2)	5	6.500
individual urine 1 (IU1)	1	7.124
individual urine 2 (IU2)	1	6.896
individual urine 3 (IU3)	1	7.180
individual urine 4 (IU4)	1	7.356
individual urine 5 (IU5)	1	6.678
individual urine 6 (IU6)	1	7.013

2.2.2 Preparation of the BDD Electrodes

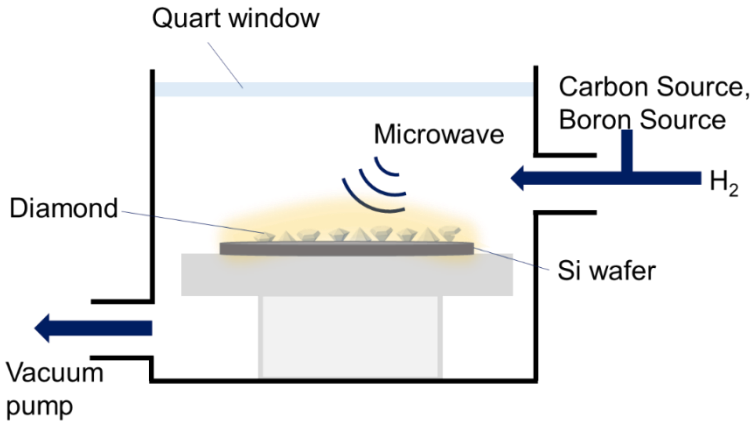

Scheme 2.1 Schematic diagram of BDD electrode fabrication under microwave plasma-assisted chemical vapor deposition.

The method of BDD preparation follows our group's previous works [29, 30] and the shown in Scheme 2.1. A single-sided silicon (100) wafer was used as the substrate. This was polished with diamond powder and washed by ultrasonication in methanol for 10 min, respectively. The BDD film was deposited onto the treated substrate using a microwave plasma-assisted chemical vapor deposition (MPCVD) system (AX6500, CORNES Technologies Corp.) with acetone and TMB as carbon and boron

sources, respectively. H_2 was used as the carrier gas. The atomic boron-carbon ratio (B/C) of the fabricated BDD was 1%. During the 4 h reaction process, the total pressure in the chamber was 115 Torr with a microwave power of 5.00 kW.

The surface morphology of the fabricated BDD electrode was recorded using a scanning electron microscope (SEM, accelerating voltage: 15.0 kV, JCM-6000, JEOL). A Raman spectrum was obtained by an Acton SP2500 (Princeton Instruments) with a 532 nm laser to confirm the successful fabrication of BDD [31].

2.2.3 Electrochemical Measurements

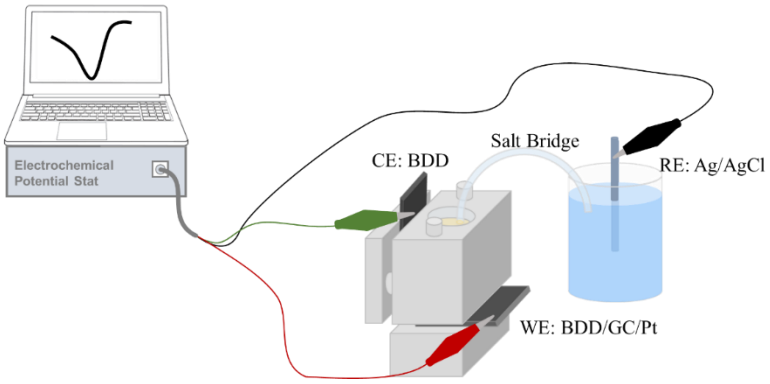

Scheme 2.2 Electrochemical reactor

Electrochemical measurements were performed using an ALS CH Instruments electrochemical analyzer (model 852Cs, CH Instruments Corp., USA) in a typical three-electrode system (Scheme 2.2). BDD, GC, and Pt electrodes were used as the working electrode (0.196 cm^2), a BDD as the counter electrode (0.363 cm^2), and Ag/AgCl (saturated 3 M KCl, Agar) electrode as the reference electrode.

The BDD electrode and reaction cell were cleaned with ultrapure water with an ultrasonic cleaner for 10 min. The BDD electrode surface was additionally cleaned by CV protocol in the range of −1.5 to 1.5 V with

a 20-cycle scan at a scan rate of 0.1 V/s in a 0.1 M PB. Before each electrochemical measurement, the BDD surface was treated with cathodic reduction (H-terminated treatment) or anodic oxidation (O-terminated treatment) by CA in a 0.1 M H_2SO_4 aqueous solution at −3.0 or +3.0 V (vs Ag/AgCl) for 5 min, respectively. About high concentration of nitrite determination, CV measurements were performed within the potential window of −1.5 to +1.5 V in PB (pH 6.4), D-PBS (pH 6.4), and human urine, respectively. The scan rate was set as 0.1 V/s, the initial potential was 0 V (vs Ag/AgCl), and the scan direction was positive, respectively. For low concentrations of $NaNO_2$ detection, CA (1.5 V, 15 s) and the DPV protocol (potential range, 0.3 to −1.0 V; increment, 0.03 V; amplitude, 0.2 V; pulse width, 0.05 s; pulse period, 0.1 s; sample width, 0.04 s) were employed for oxidation and reduction, respectively, in both pooled and individual urine.

2.2.4 Data Analysis

Microsoft Excel and Origin software were used to analyze the obtained data from the electrochemical and Raman spectra measurements. A $NaNO_2$ limit of detection (LOD) value in real urine samples was calculated based on the DPV cathodic reduction currents of five urine samples. The values of the difference between the currents at −0.45 and 0 V were used to normalize different urine samples. The LOD value calculation is based on the calibration curve and described in eq 1 [32]

$$LOD = 3.3\ \sigma/S \quad (1)$$

σ is the standard deviation of y-intercepts of regression lines and S is the absolute value of the slope of the calibration curve in Figure 2.15 B.

2.3 Results and Discussion

2.3.1 Characterization

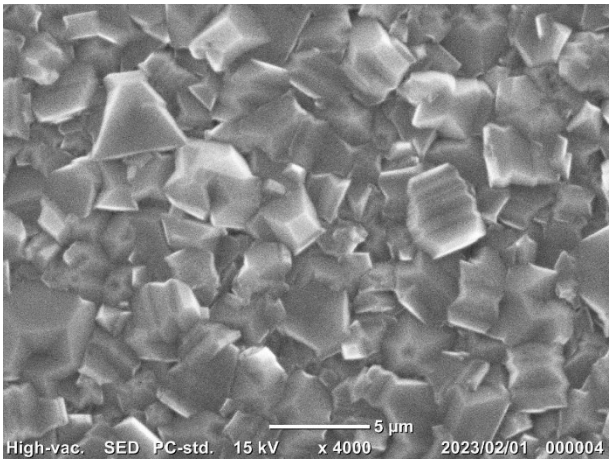

Figure 2.1 SEM image of BDD electrode. Reproduced from ref. [33].

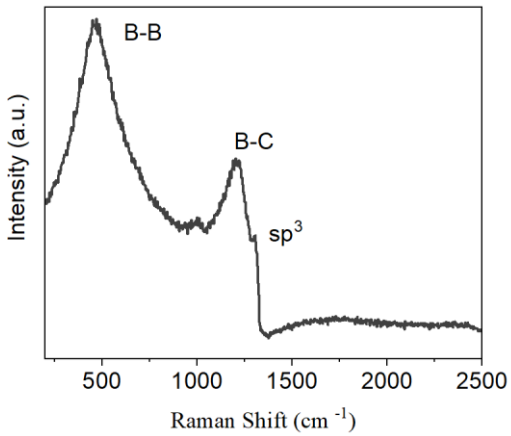

Figure 2.2 Raman spectrum of the BDD electrode. Reproduced from ref. [33].

The surface morphology of the BDD electrode was confirmed using a scanning electron microscope (SEM). As shown in Figure 2.1 [33], the grain sizes of the polycrystalline diamond were around 2−5µM, which correspond well to our group previous work [34]. As could be seen in Figure 2.2, a well-defined peak at 1300 cm^{-1} is ascribed to the existence of

sp^3 carbon bonds in Raman spectra. The other two peaks located at around 500 and 1200 cm^{-1} can be assigned to the typical vibrations of the B-B and B-C pairs, respectively, which indicate the boron doping in the diamond structure. These observations illustrate the fabricated BDD was of superior quality.

2.3.2 Optimization on Surface Termination of BDD Electrode

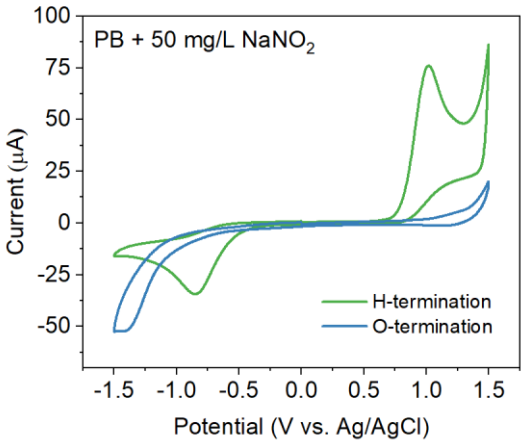

Figure 2.3. CV properties of $NaNO_2$ on different surface terminated BDD. CV measurement of 0.1 M PB with 50 mg/L $NaNO_2$. Potential window: –1.5 V to +1.5 V, scan rate: 0.1 V/s, initial potential: 0 V, initial potential direction: positive. Reproduced from ref. [33].

The surface termination pretreatments, which can enhance the sensitivity and selectivity of measurements [35, 36], were performed on the bare BDD (Figure 2.3). The results clearly revealed that the BDD electrode with an H-terminated surface exhibits a higher current response for $NaNO_2$ than that of the O-termination due to the higher conductivity of the H-terminated surface BDD [37, 38].

2.3.3 Detection of $NaNO_2$ on Different Electrodes

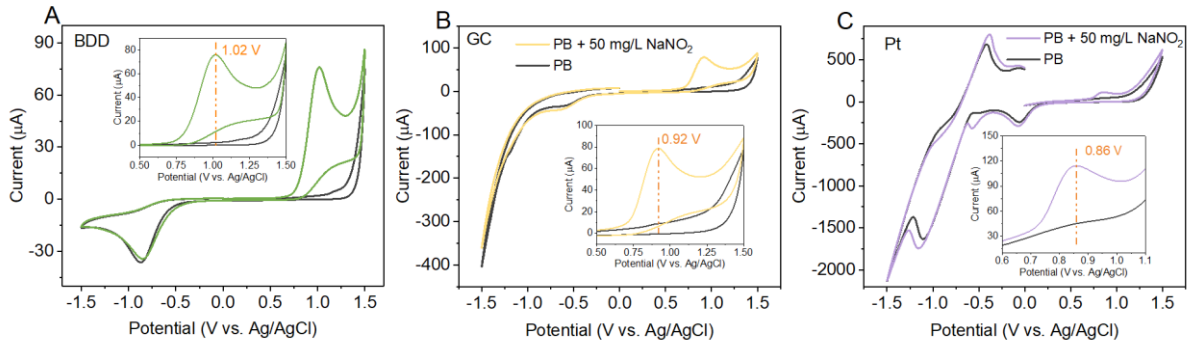

Figure 2.4. CV properties of $NaNO_2$ on different electrodes. CV measurement of 50 mg/L $NaNO_2$ in 0.1 M PB using different working electrodes: **A** H-terminated BDD; **B** glassy carbon (GC); **C** platinum (Pt) electrode; Insets: an expanded version of the CV test of $NaNO_2$ oxidation peak on each electrode. Potential window: –1.5 V to +1.5 V, scan rate: 0.1 V/s, initial potential: 0 V, initial potential direction: positive. Reproduced from ref. [33].

Table 2.2. The ratio of $NaNO_2$ electrochemical response signal to background on different electrodes. Reproduced from ref. [33].

Electrodes	BDD	GC	Pt
S/B	35.8	8.81	2.54

The CVs of $NaNO_2$ in PB on different electrodes are shown in Figure 2.4. The calculated signal-to-background (S/B) ratios of the BDD, GC, and Pt electrodes were 35.8, 8.81, and 2.54, respectively (Table 2.2). These results indicate the higher electrochemical sensitivity of BDD than other electrodes.

2.3.4 Detection of $NaNO_2$ on BDD Electrode

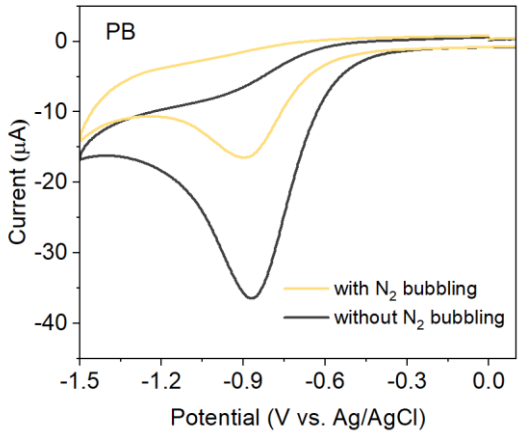

Figure 2.5. N_2 bubbling effect in PB. CV measurements of 0.1 M PB at H-terminated BDD electrode before (black) and after (yellow) N_2 bubbling. Potential window: −1.5 V to +1.5 V, scan rate: 0.1 V/s, initial potential: 0 V, initial potential direction: positive. Reproduced from ref. [33].

The CV of 0.1 M PB with and without 50 mg/L $NaNO_2$ on a bare BDD electrode is shown in Figure 2.4 A. Two well-defined peaks at 1.0 V (vs Ag/AgCl) and −0.87 V (vs Ag/AgCl) are observed. The peak at 1.0 V is assigned to the oxidation of $NaNO_2$ [21, 39]. Because the reduction peak at −0.87 V was decreased by N_2 bubbling (Figure 2.5), it was assigned to the dissolved oxygen [40, 41]. This result indicates that $NaNO_2$ has electrochemical oxidation activity in PB when using a BDD electrode.

2.3.4.1 Electrochemical Performance of $NaNO_2$ in the Positive Potential Range

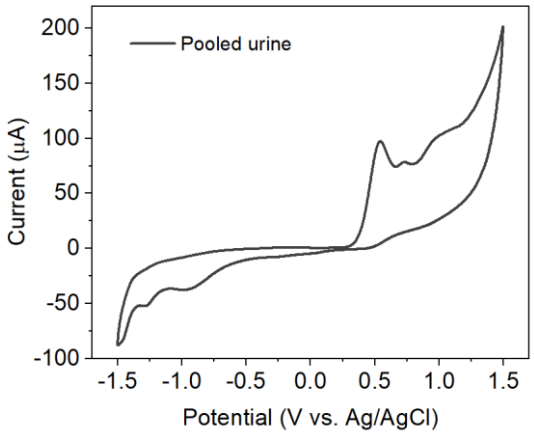

Figure 2.6. CV response of human urine. CV measurement of pooled urine 1 at H-terminated BDD electrode. Potential window: −1.5 V to +1.5 V, scan rate: 0.1 V/s, initial potential: 0 V, initial potential direction: positive. Reproduced from ref. [33].

A CV measurement of human pooled urine is shown in Figure 2.6. Several anodic current responses from 0.27 to 1.5 V (vs Ag/AgCl) were attributed to the oxidation of multiple nutrients and endogenous substances in the urine. Furthermore, due to the extreme complexity of human urine composition and individual differences [28], there would be obvious distinctions among individual urine samples. Moreover, $NaNO_2$ electrochemical oxidation on the BDD electrode occurs around 1.0−1.2 V [39] (Figure 2.4 A), and therefore these nonignorable anodic electrochemical signal responses from 0.27 to 1.5 V indicate the difficulty of obtaining a pure or uniform electrochemical background signal for $NaNO_2$ detection in different human urine samples without further treatment, which greatly restricts the general application of $NaNO_2$ detection in real urine in terms of quick UTI self-monitoring. Since the oxidation of $NaNO_2$ is likely affected by different background currents in

human urine, it is inevitable to instead consider detecting nitrite in a region where there is little difference in the background currents of various samples. Therefore, a cathodic reduction range was taken into consideration.

2.3.4.2 Electrochemical Performance of $NaNO_2$ in the Negative Potential Range in D-PBS

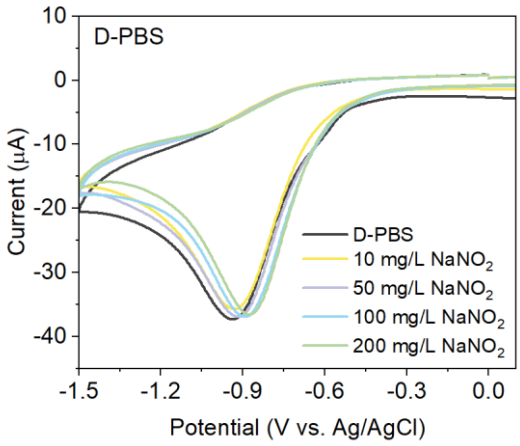

Figure 2.7. Electrochemical performance of $NaNO_2$ in D-PBS. CV measurements of different concentrations of $NaNO_2$ in D-PBS (pH=6.4) at the H-terminated BDD electrode. Potential window: −1.5 V to +1.5 V, scan rate: 0.1 V/s, initial potential: 0 V, initial potential direction: positive. Reproduced from ref. [33].

The electrochemical performance of $NaNO_2$ in D-PBS was evaluated by CV measurement in the cathodic reduction range, as shown in Figure 2.7. In D-PBS, the reduction peak was observed at −0.94 V (vs Ag/AgCl), which was due to the reduction of dissolved oxygen [42]. The peaks shifted to a slightly more positive direction with the addition of $NaNO_2$, implying the adsorption of $NaNO_2$ or its related oxidation products on the BDD surface. In contrast, no apparent cathodic reduction current variation was observed with the addition of $NaNO_2$, indicating that it is difficult to detect $NaNO_2$ solely based on the cathodic reduction current in D-PBS.

2.3.4.3 Electrochemical Performance of High Concentrations of $NaNO_2$ in the Negative Potential Range in Human Urine

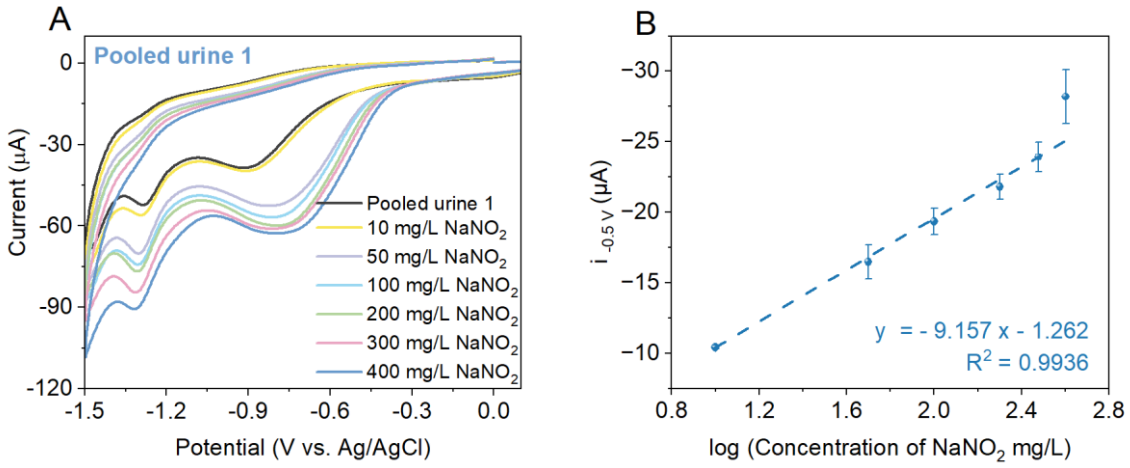

Figure 2.8. Detection of $NaNO_2$ in pooled urine. (A) CV measurements of different concentrations of $NaNO_2$ in pooled urine 1 at H-terminated BDD electrode. (B) Calibration plot of reduction current at −0.5 V (vs Ag/AgCl) and the logarithm of $NaNO_2$ concentration. Reproduced from ref. [33].

Pooled urine from several donors with added concentrations of 10−400 mg/L $NaNO_2$ was tested. The CV response of pooled urine 1 contained two well-defined reduction peaks in the negative potential range (Figure 2.8 A). The broad peak at around −0.92 V (vs Ag/AgCl) is also assigned to dissolved oxygen. In addition, with the increasing concentration of $NaNO_2$, the cathodic reduction of dissolved oxygen shifted to a positive direction gradually, which corresponds to the behavior in D-PBS. Another reduction peak observed at around −1.29 V (vs Ag/AgCl) is associated with the reduction of certain endogenous substances in urine or their oxidation products.

Most importantly, the cathodic reduction current value of pooled urine 1 increased with the addition of $NaNO_2$ in the range of −1.5 to −0.3 V (vs Ag/AgCl). Here, the calibration curve between the current values observed at −0.5 V and the logarithm of the $NaNO_2$ concentration was established successfully with a coefficient of determination (R^2) of 0.9936. This observation greatly enhanced the possibility of $NaNO_2$ detection in human pooled urine (Figure 2.8 B). Although this behavior does not satisfy typical Bard's diffusion regulation [43], it could be ascribed to complex substances in human urine absorbed on the BDD electrode.

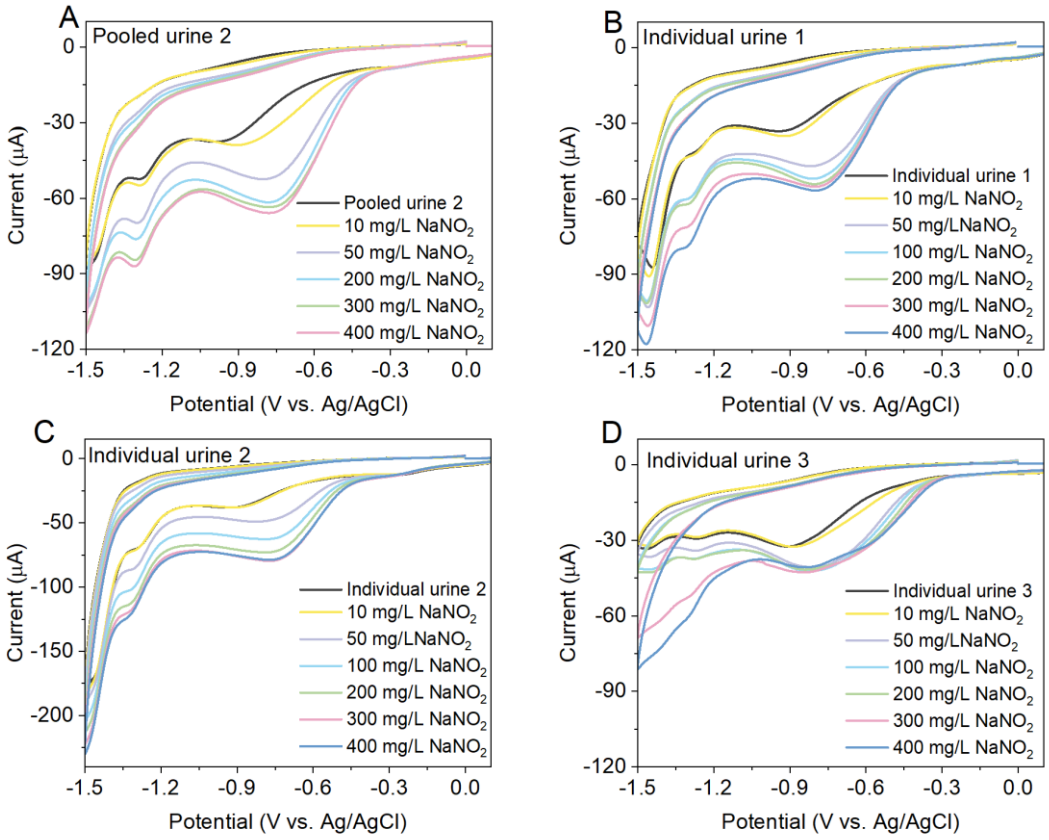

Figure 2.9. CV performance of high concentration of $NaNO_2$ in different urine samples. Cyclic voltammetry measurement of $NaNO_2$ at H-terminated BDD electrode in different urine: **A** pooled urine 2, **B** individual urine 1, **C** individual urine 2, **D** individual urine 3. Potential window: −1.5 V to +1.5 V, scan rate: 0.1 V/s, initial potential: 0 V, initial potential direction: positive. Reproduced from ref. [33].

Note that the $NaNO_2$ concentration dependence of the current values was not observed in D-PBS (Figure 2.7) while it was observed in human pooled urine (Figure 2.8 A). This inconsistency was ascribed to the existence of some components in urine that react with $NaNO_2$, the products of which were electrochemically active.

To investigate the universality of the linear relationship between concentration and cathodic reduction current difference in various urine samples, another pooled urine and three other individual urine samples were also measured by CV (Figure 2.9 A−D). The results showed that a regular variation of the reduction current around −0.5 V occurred as the added $NaNO_2$ concentration increased in most of the urine samples. This phenomenon, which appears in all urine samples but not in D-PBS indicates that the detection of nitrite in our system does not depend on its direct electrochemical redox. There may be certain common substances in human urine that would react with nitrite, and then their product is electrochemically active and could be reduced at around −0.5 V (vs Ag/AgCl). These results demonstrated that it is possible to detect $NaNO_2$ in different human urine using a simple electrochemical method without adding any other chemicals. However, significant distinctions in the shape of the reduction current were observed in the negative range, which was attributed to different components and concentrations within the urine samples.

2.3.4.4 Normalization in Different Urine Samples.

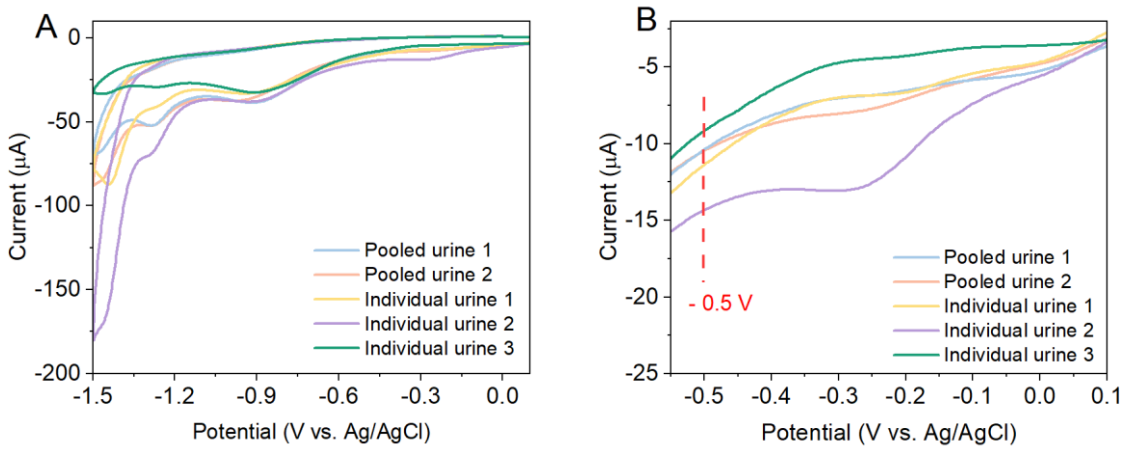

Figure 2.10. Electrochemical response for different urine. A CV measurement of different urine samples: pooled urine 1, pooled urine 2, individual urine 1, individual urine 2, and individual urine 3 on H-terminated BDD electrode and **B** expanded version of CV results. Reproduced with from ref. [33].

Figure 2.10 A, B shows the apparent differences among urine samples in the cathodic reduction region, especially at −0.5 V (vs Ag/AgCl) in three individual urine samples. Due to this variation, it is necessary to find an effective method to normalize different urine samples. To further suppress the distinct background currents and realize the normalization in various urine samples, the value of the "subtraction current" between −0.5 and 0 V (vs Ag/AgCl) was chosen due to the absence of a $NaNO_2$ relative reaction Faradaic response at 0 V (vs Ag/AgCl), as seen in Figure 2.7. Furthermore, linear fittings were successfully performed between the cathodic reduction current difference between −0.5 and 0 V (vs Ag/AgCl) and the logarithm of $NaNO_2$ concentration in the urine samples. The calibration curves and the equations of $NaNO_2$ measurement in different human urine samples are

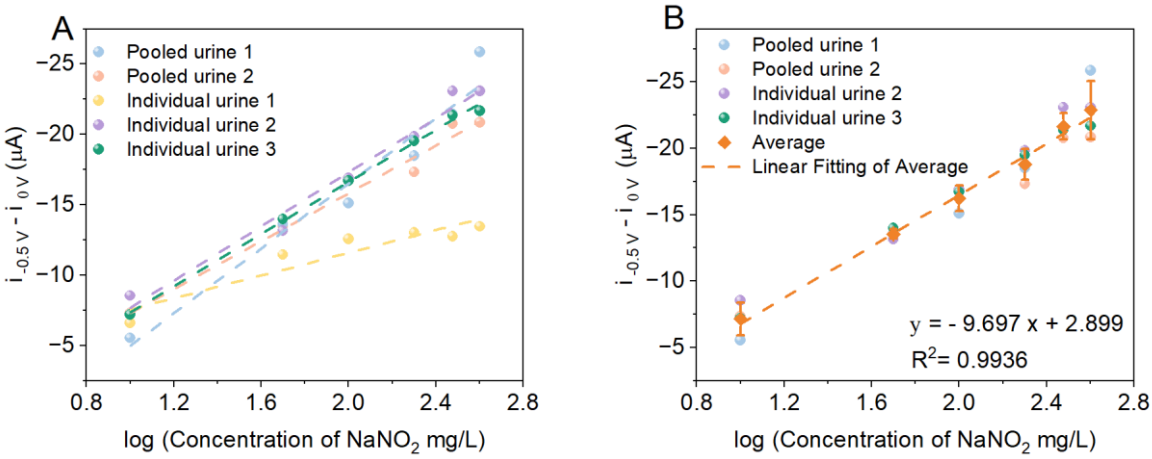

Figure 2.11. Normalization of different urine samples. A Calibration plot of the reduction current difference between −0.5 and 0 V (vs Ag/ AgCl) and the logarithm of $NaNO_2$ concentration in different urine samples: pooled urine 1, pooled urine 2, individual urine 1, individual urine 2, and individual urine 3 and **B** the normalization of 10−400 mg/L $NaNO_2$ in different urine samples: pooled urine 1, pooled urine 2, individual urine 2, individual urine 3, and average of these four urine samples. Reproduced from ref. [33].

Table 2.3. Fitting equations of different urine samples with spiked $NaNO_2$ from 10−400 mg/L (140−5800 µmol/L) using the normalization method. Reproduced from ref. [33].

Urine samples	Equation y= a logx + b		
	Slope: a	Intercept: b	R^2
Pooled urine 1	−11.54	6.544	0.9556
Pooled urine 2	−8.504	1.193	0.9849
Individual urine 1	−4.034	−3.521	0.8786
Individual urine 2	−9.608	1.911	0.9795
Individual urine 3	−9.262	1.902	0.9972

shown in Figure 2.11 A and Table 2.3, respectively. It is clearly shown that a linear relationship exists in both pooled samples and individual urine. The results demonstrated that the $NaNO_2$ concentration measurement

could be fulfilled by a simple electrochemical behavior on the BDD electrode surface in different human urine samples.

Obtaining a uniform standard equation for different urine samples is crucial for the general application of $NaNO_2$ determination in different human urine samples. It is worth mentioning that with the help of the "subtraction current", four kinds of urine could be converted into the same equation with R^2 as 0.9936 (Figure 2.11 B). This result exhibits great potential for this simple electrochemical strategy for $NaNO_2$ detection using a BDD electrode in complex urine matrices. Only individual urine 1 sample was hard to normalize to the same equation due to the presence of ascorbic acid contained in this urine. Ascorbic acid is recognized as a common reason for a decline in the accuracy of substance detection in urine [44]. In addition, an apparent oxidation current at around 0.25 V (vs. Ag/AgCl) could be easily observed in individual urine 1 compared with other urine samples (Figure 2.12). Ascorbic acid can be oxidized at a

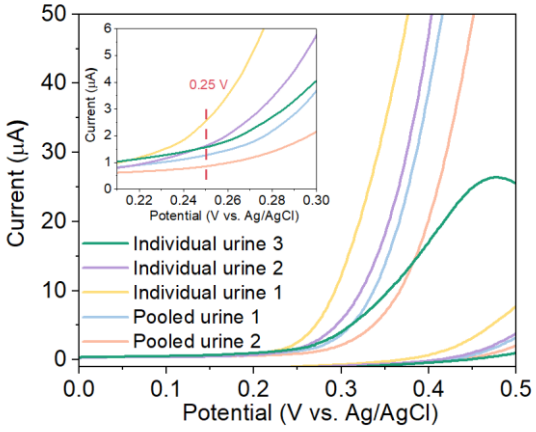

Figure 2.12. CV response for different urine samples. CV measurements of different urine samples: pooled urine 1, pooled urine 2, individual urine 1, individual urine 2, individual urine 3 at H-terminated BDD electrode. Inset: expansion in area 0.2 to 0.3 V (vs. Ag/AgCl). Potential window: −1.5 V to +1.5 V, scan rate: 0.1 V/s, initial potential: 0 V, initial potential direction: positive. Reproduced from ref. [33].

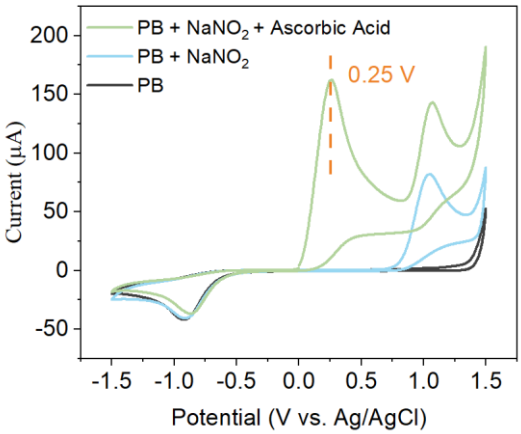

Figure 2.13. CV performance of ascorbic acid in PB. CV measurements of 50 mg/L $NaNO_2$ with and without 0.5 g/L ascorbic acid at H-terminated BDD electrode in 0.1 M PB. Potential window: −1.5 V to +1.5 V, scan rate: 0.1 V/s, initial potential: 0 V, initial potential direction: positive. Reproduced from ref. [33].

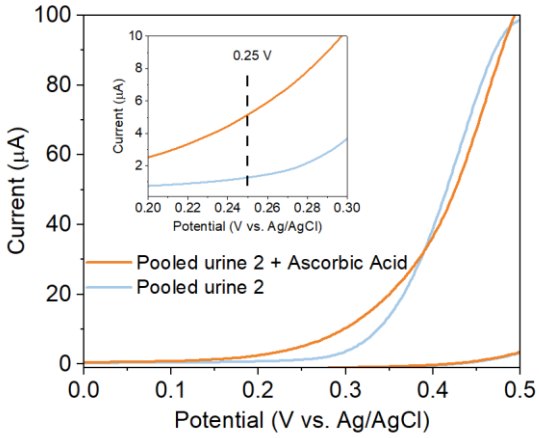

Figure 2.14. CV performance of added ascorbic acid in pooled urine. CV measurements of pooled urine 1 with and without 50 mg/L ascorbic acid at H-terminated BDD electrode. Inset: expansion in area 0.2 to 0.3 V (vs. Ag/AgCl). Potential window: −1.5 V to +1.5 V, scan rate: 0.1 V/s, initial potential: 0 V, initial potential direction: positive. Reproduced with permission from ref. [33].

similar potential on the BDD electrode (Figure 2.13). We note that after the addition of ascorbic acid directly into pooled urine 1, the oxidation current was also enhanced (Figure 2.14). The results revealed that it is possible to

directly detect $NaNO_2$ in human urine with an electrochemical oxidation step followed by a reduction approach using a bare BDD electrode in a negative potential range. However, serious consideration needs to be given to the results if an excessive amount of ascorbic acid intake has taken place.

2.3.4.5 Electrochemical Performance of Low Concentrations of $NaNO_2$ in the Negative Potential Range in Human Urine

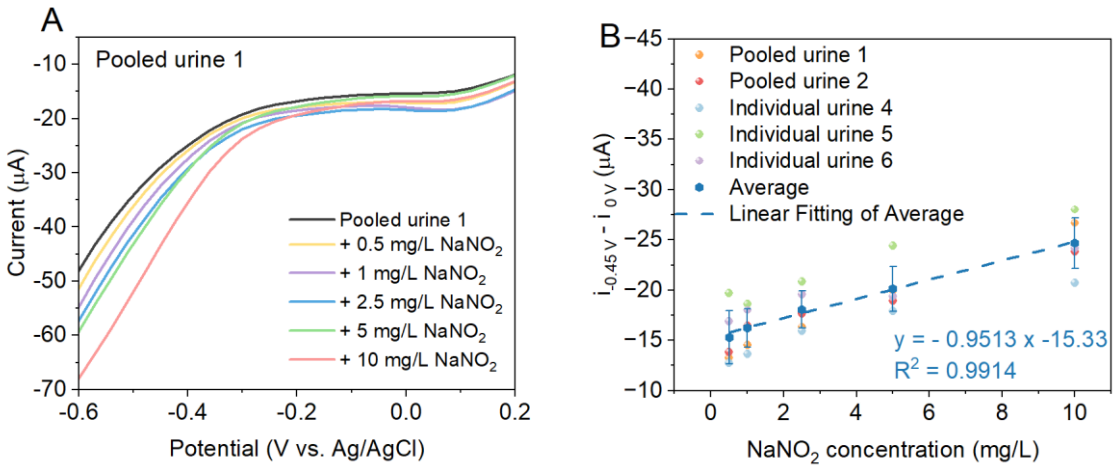

Figure 2.15 Low concentrations $NaNO_2$ detection in urine. (A) DPV measurements of 0.5−10 mg/L $NaNO_2$ in pooled urine 1 using a H-terminated BDD electrode and (B) the normalization of 0.5−10 mg/L $NaNO_2$ in different urine samples: pooled urine 1, pooled urine 2, individual urine 4, individual urine 5, individual urine 6, and average of these five urine samples. Reproduced with permission from ref. [33].

Even a low concentration of $NaNO_2$ in human urine may indicate the presence of UTIs in the urinary system. The low concentration $NaNO_2$ measurement can be accomplished by the following steps: begin with the CA (1.5 V, 15 s) for oxidation and then reduction by DPV (potential range, 0.3 to −1.0 V; increment, 0.03 V; amplitude, 0.2 V; pulse width, 0.05 s; pulse period, 0.1 s; sample width, 0.04 s). As shown in Figures 2.15 A and

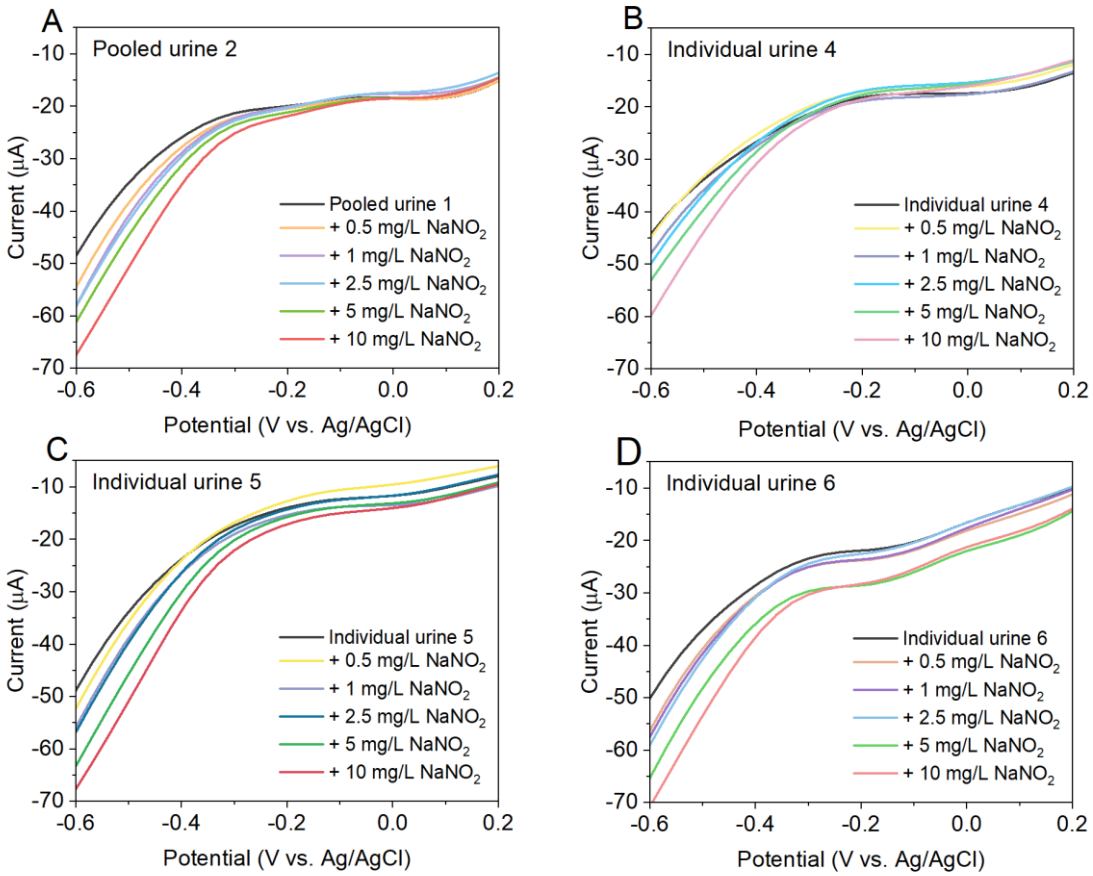

Figure 2.16. DPV performance of low concentration of $NaNO_2$ in different urine samples at H-terminated BDD electrode. A pooled urine 2, B individual urine 4, C individual urine5, D individual urine 6. (Potential window 0.3 to −1.0 V, increment, 0.03 V; amplitude, 0.2 V; pulse width, 0.05 s; pulse period, 0.1 s; sample width, 0.04 s). Reproduced from ref. [33].

2.16 A−D, the apparent current variations could be observed in the pooled and individual urine samples. Normalization in different urine samples was fulfilled using the "subtraction current" between −0.45 and 0 V (vs Ag/AgCl) to obtain a better LOD and good linearity of the calibration curves. A linear calibration curve between the $NaNO_2$ concentration and the average of the subtraction currents in these five kinds of urine was achieved with a LOD of 0.82 mg/L and an R^2 value of 0.9914 (Figure 2.15 B).

The successful measurement of low concentrations of $NaNO_2$ using a

bare BDD electrode in different urine samples with a simple electrode approach could be particularly important for diagnostic applications. The linear range of $NaNO_2$ concentration in human urine by this method is 0.5−10 mg/L and the LOD is 0.82 mg/L. In addition, this method is based on a direct measurement of the urine sample and has a wider detection range than that of the dipstick method [45]. In our approach, color distinguishing with the naked eye is no longer necessary and the concentration of $NaNO_2$ in urine can be obtained directly. This is beneficial for the long-term monitoring of changes in UTIs and for the resulting medication guidance.

2.3.4.6 Interference Study

Human urine contains nearly 3000 kinds of compounds. It is complicated to confirm all of the species in human urine. Some representative compounds in urine, such as urea, glucose, creatinine, and uric acid, are added into PB, respectively. As shown in Figures 2.17 and 2.18, the reduction currents did not change obviously with the addition of creatinine, urea and glucose. The reduction currents of different concentrations of uric acid at 0 V exhibit regular change (Figure 2.17 D). In our experiments, we used the subtraction current between −0.5 (or −0.45) and 0 V. This means we can use this subtraction to eliminate or reduce the error caused by different uric acid contents in urine samples.

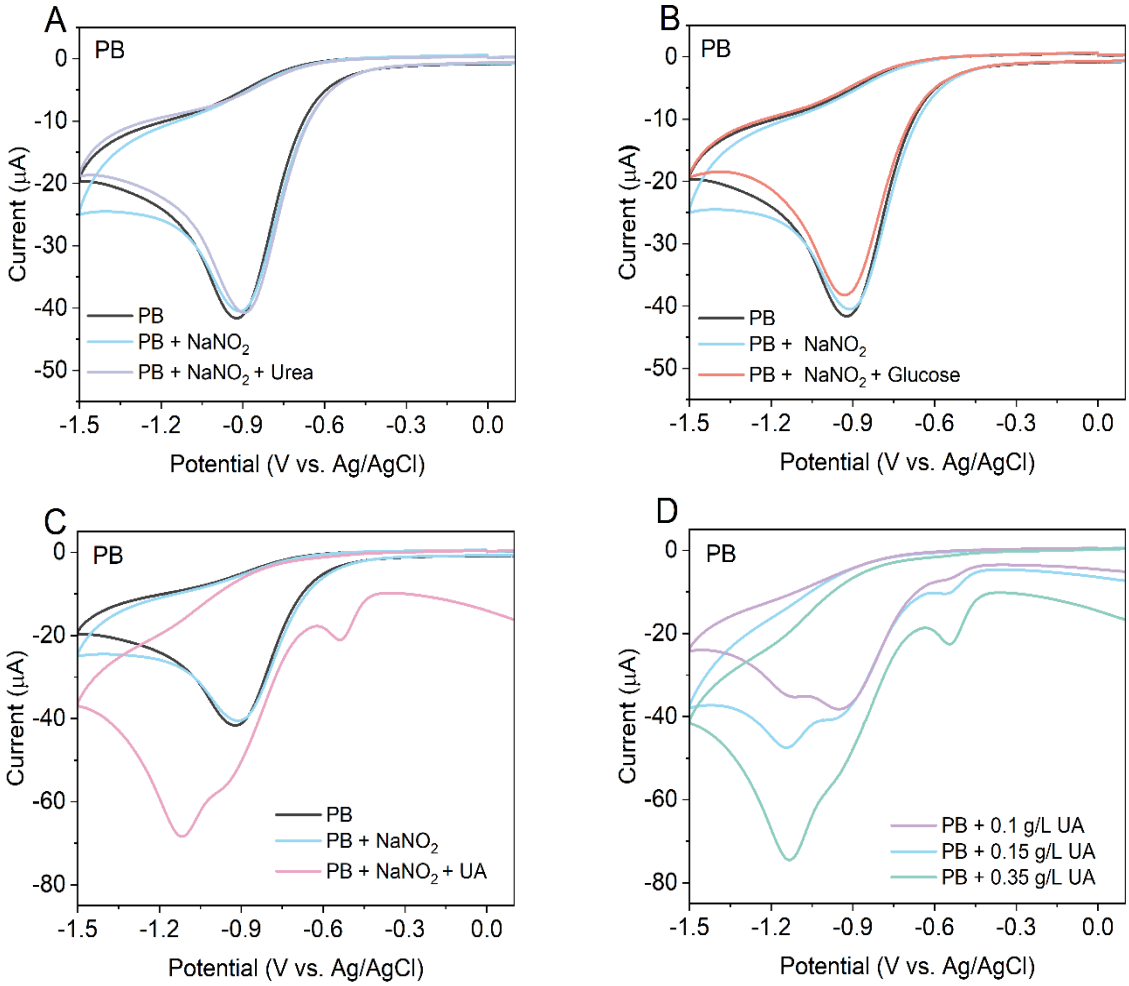

Figure 2.17. CV performance of urea, glucose and uric acid in PB. CV measurements of 50 mg/L $NaNO_2$ with and without **A** 25 g/L urea; **B** 0.2 g/L glucose; C 0.35g/L uric acid and D CV measurements of different concentration of uric acid at H-terminated BDD electrode in 0.1 M PB. Potential window: −1.5 V to +1.5 V, scan rate: 0.1 V/s, initial potential: 0 V, initial potential direction: positive. Reproduced from ref. [33].

2.3.4.7 Possible Mechanism for the Electrochemical $NaNO_2$ Detection in Human Urine

We speculate that both creatinine and Cl^- ions in human urine are necessary for electrochemical $NaNO_2$ detection. Control experiments in PB (absence of Cl^-, Figure 2.18) or D-PBS (absence of creatinine, Figure 2.7) did not show any distinguishable Faradaic response variation at −0.5

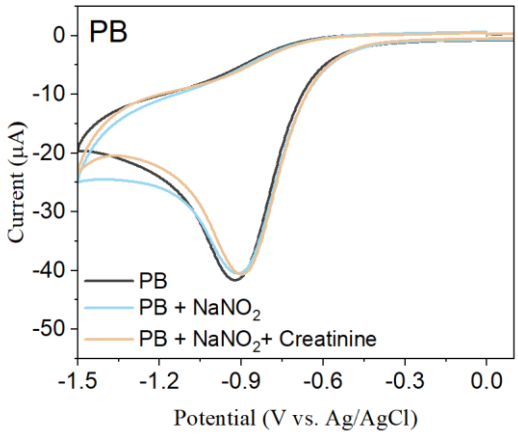

Figure 2.18. CV properties of creatinine in PB. CV measurements of 50 mg/L $NaNO_2$ with and without 0.2 g/L creatinine in 0.1 M PB at H-terminated BDD electrode. Potential window: −1.5 V to +1.5 V, scan rate: 0.1 V/s, initial potential: 0 V, initial potential direction: positive. Reproduced from ref. [33].

V with the addition of $NaNO_2$, and a significant linear relationship in urine was not observed in these experimental results. On the contrary, $NaNO_2$ detection with creatinine in D-PBS which contains Cl^- was obtained in Figure 2.19 A. A small but clear cathodic reduction peak around −0.5 V (vs Ag/AgCl) was observed with the addition of $NaNO_2$ concentrations.

Furthermore, the calculation results have demonstrated a correlation between the reduction current difference and the concentration of $NaNO_2$ in D-PBS containing creatinine (Figure 2.19 B) with an R^2 at 0.9875, although the linear fitting was not based on the logarithm of the $NaNO_2$ concentration, which can be ascribed to the intrinsic difference between this simulate solution and urine. In addition, the adsorption and diffusion of compounds in urine would be different from that in D-PBS.

The plausible reaction pathways are shown in Scheme 2.3. The solution was first oxidized at 1.5 V (vs Ag/AgCl). The proton is generated by water oxidation under this potential and is involved in the subsequent diazotization reaction. $NaNO_2$ and Cl^- under the acidic condition, would react with the primary amine group of creatinine to generate a diazonium

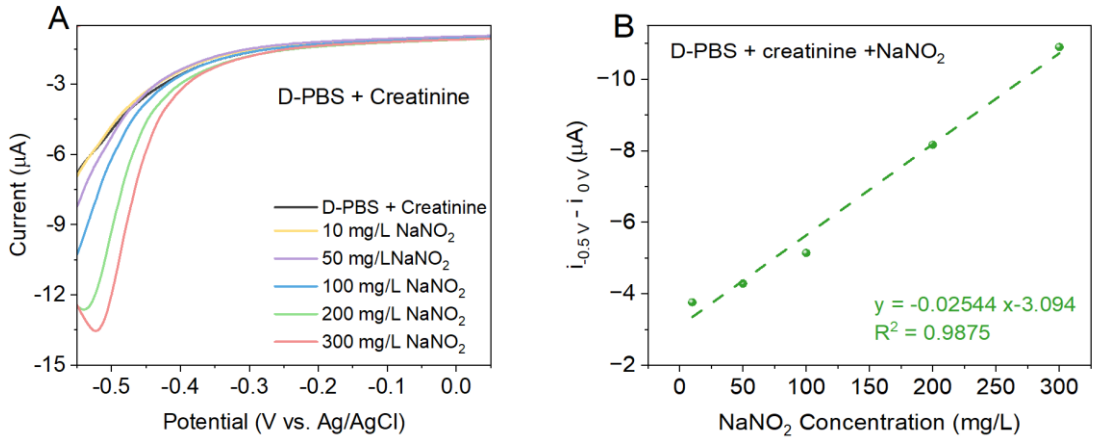

Figure 2.19 Detection of $NaNO_2$ under the existence of creatinine in D-PBS. A, CV measurements of $NaNO_2$ with 2.0 g/L creatinine at BDD electrode in 0.1 M D-PBS at H-terminated BDD electrode. Potential window: −1.5 V to +1.5 V, scan rate: 0.1 V/s, initial potential: 0 V, initial potential direction: positive. B, Calibration plot of the reduction current difference between −0.5 and 0 V (vs. Ag/AgCl) and the logarithm of $NaNO_2$ concentration. Reproduced from ref. [33].

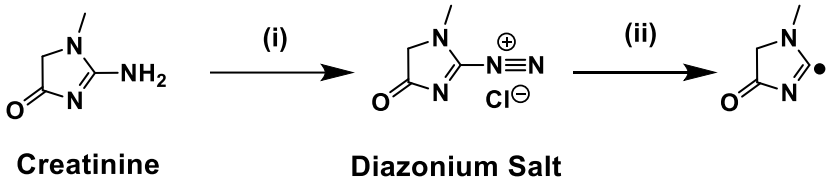

(i) $NaNO_2$, Cl^- and H^+ generated by water oxidation
(ii) Electrochemical reduction

Scheme 2.3. Plausible reaction pathways of $NaNO_2$ detection in urine sample. Reproduced from ref. [33].

salt [46]. Then the diazonium salt was electrochemically reduced irreversibly to the radical species. Such a reduction process involves no hydrogen ions and would exhibit no variation in the potential peak position with pH [47]. Therefore, this $NaNO_2$ detection method can be widely used in various urine samples with pH values ranging from 6.5 to 7.3, which is in the range of normal urine [28]. Furthermore, the reaction mechanism demonstrates another advantage of this method as Cl^- and creatinine are endogenous compounds of human urine, and it is not necessary to add

extra chemicals to generate the proposed reaction.

2.4 Conclusion

The fast electrochemical detection of $NaNO_2$ in human urine was successfully achieved by using CV, CA, and DPV measurements with a bare BDD electrode. Cathodic reduction currents were used to decrease the influence of different background currents in the urine samples. To realize the normalization of different samples in the high concentration range (10−400 mg/L), we have developed a urinary $NaNO_2$ sensor that has a linear relationship between the cathodic reduction current difference between −0.5 and 0 V (vs Ag/ AgCl) and the logarithm of $NaNO_2$ concentration. Most of the pooled and individual urine samples converted well into a uniform standard equation with R^2 as 0.9936. Only one individual urine sample was hard to normalize into the same equation due to the presence of ascorbic acid in that urine sample. In the low concentration range (0.5−10 mg/L), the subtraction value of the DPV reduction current between −0.45 and 0 V (vs Ag/AgCl) and $NaNO_2$ concentration was employed to construct a calibration curve with a LOD at 0.82 mg/L and with R^2 at 0.9914. In investigating the reaction mechanism for $NaNO_2$ detection, we propose that the in situ generated diazonium salt from creatinine and Cl^-, which are endogenous substances in the urine, plays an essential role in the electrochemical measurement of $NaNO_2$.

In summary, an affordable, sensitive, rapid, and simple method for measuring $NaNO_2$ in different human urine samples is fulfilled by an electrochemical approach using a BDD electrode with an oxidation step, followed by reduction without adding any other chemicals. In this process, the urinary nitrite concentration could be calculated from the uniform equation based on its reduction current. The approach can be user-friendly

in terms of self-monitoring the abnormal $NaNO_2$ in urine or the changes due to a UTI and would be helpful for family health management in the future, especially under resource-limited conditions. Importantly, it also presents a significant aid to clinical research for the assessment of the risk of UTIs and to provide the appropriate medical guidance. However, the intake of foods, fruits, and medicines containing a large amount of ascorbic acid will have an impact on the test results, and caution in interpretation is required in these conditions.

2.5 Reference

[1] Gupta, K.; Grigoryan, L.; Trautner, B. Urinary tract infection. *Ann. Intern. Med.* **2017**, 167, ITC49-ITC64.

[2] Masajtis-Zagajewska, A.; Nowicki, M. New markers of urinary tract infection. *Clin. Chim. Acta* **2017**, 471, 286-291.

[3] Chu;, C. M.; Lowder, J. L. Diagnosis and treatment of urinary tract infections across age groups. *Am. J. Obstet. Gynecol.* **2018**, 219, 40-51.

[4] Koeijers, J. J.; Kessels, A. G.; Nys, S.; et al. Evaluation of the nitrite and leukocyte esterase activity tests for the diagnosis of acute symptomatic urinary tract infection in men. *Clin. Infect. Dis.* **2007**, 45, 894-896.

[5] Juthani‐Mehta, M.; Tinetti, M.; Perrelli, E.; et al. Role of dipstick testing in the evaluation of urinary tract infection in nursing home residents. *Infect. Control Hosp. Epidemiol.* **2007**, 28, 889-891.

[6] Lachs, M. S.; Nachamkin, I.; Edelstein, P. H.; et al. Spectrum bias in the evaluation of diagnostic tests: Lessons from the rapid dipstick test for urinary tract infection. *Ann. Intern. Med.* **1992**, 117, 135-140.

[7] Williams, G. J.; Macaskill, P.; Chan, S. F.; et al. Absolute and relative accuracy of rapid urine tests for urinary tract infection in children: A

meta-analysis. *Lancet Infect. Dis.* **2010**, 10, 240-250.

[8] Masic, A.; Santos, A. T.; Etter, B.; et al. Estimation of nitrite in source-separated nitrified urine with uv spectrophotometry. *Water Res.* **2015**, 85, 244-254.

[9] Burakham, R.; Oshima, M.; Grudpan, K.; et al. Simple flow-injection system for the simultaneous determination of nitrite and nitrate in water samples. *Talanta* **2004**, 64, 1259-1265.

[10] Mikuška, P.; Večeřa, Z. Simultaneous determination of nitrite and nitrate in water by chemiluminescent flow-injection analysis. *Anal. Chim. Acta* **2003**, 495, 225-232.

[11] Tsikas, D. Simultaneous derivatization and quantification of the nitric oxide metabolites nitrite and nitrate in biological fluids by gas chromatography/mass spectrometry. *Anal. Chem.* **2000**, 72, 4064-4072.

[12] Tsikas, D.; Boger, R. H.; Bode-Boger, S. M.; et al. Quantification of nitrite and nitrate in human urine and plasma as pentafluorobenzyl derivatives by gas chromatography-mass spectrometry using their ^{15}n-labelled analogs. *J. Chromatogr. B* **1994**, 661, 185-191.

[13] Wang, X.; Adams, E.; Van Schepdael, A. A fast and sensitive method for the determination of nitrite in human plasma by capillary electrophoresis with fluorescence detection. *Talanta* **2012**, 97, 142-144.

[14] Gaspar, A.; Juhasz, P.; Bagyi, K. Application of capillary zone electrophoresis to the analysis and to a stability study of nitrite and nitrate in saliva. *J. Chromatogr. A* **2005**, 1065, 327-331.

[15] Guo, Y. X.; Zhang, Q. F.; Shangguang, X.; et al. Spectrofluorimetric determination of trace nitrite with o-phenylenediamine enhanced by hydroxypropyl-beta-cyclodextrin. *Spectrochim. Acta A Mol. Biomol. Spectrosc.* **2013**, 101, 107-111.

[16] Afkhami, A.; Soltani-Felehgari, F.; Madrakian, T.; et al. Surface decoration of multi-walled carbon nanotubes modified carbon paste

electrode with gold nanoparticles for electro-oxidation and sensitive determination of nitrite. *Biosens. Bioelectron.* **2014**, 51, 379-385.

[17] Fu, L.; Yu, S.; Thompson, L.; et al. Development of a novel nitrite electrochemical sensor by stepwise in situ formation of palladium and reduced graphene oxide nanocomposites. *RSC. Adv.* **2015**, 5, 40111-40116.

[18] Liu, M.; Zhang, S.; Gao, J.; et al. Enhanced electrocatalytic nitrite determination using poly(diallyldimethylammonium chloride)-coated $Fe_{1.833}(OH)_{0.5}O_{2.5}$-decorated N-doped graphene ternary hierarchical nanocomposite. *Sens. Actuat. B Chem.* **2017**, 243, 184-194.

[19] Kung, C.-W.; Chang, T.-H.; Chou, L.-Y.; et al. Porphyrin-based metal–organic framework thin films for electrochemical nitrite detection. *Electrochem. Commun.* **2015**, 58, 51-56.

[20] Zhuang, J.; Pan, H.; Feng, W. 3D urchin–like CoVO/MXene nanosheet composites for enhanced detection signal of nitrite. *Sens. Actuat. B Chem.* **2023**, 378, 133207.

[21] Feng, X.; Han, G.; Cai, J.; et al. Au@carbon quantum dots-MXene nanocomposite as an electrochemical sensor for sensitive detection of nitrite. *J. Colloid Interface Sci.* **2022**, 607, 1313-1322.

[22] Muthumariappan, A.; Govindasamy, M.; Chen, S.-M.; et al. Screen-printed electrode modified with a composite prepared from graphene oxide nanosheets and Mn_3O_4 microcubes for ultrasensitive determination of nitrite. *Mikrochim. Acta* **2017**, 184, 3625-3634.

[23] Kung, C. W.; Li, Y. S.; Lee, M. H.; et al. In situ growth of porphyrinic metal–organic framework nanocrystals on graphene nanoribbons for the electrocatalytic oxidation of nitrite. *J. Mater. Chem. A* **2016**, 4, 10673-10682.

[24] Li, C.; Guo, B.; Guo, X. M.; et al. The electrochemical sensor based on electrochemical oxidation of nitrite on metalloporphyrin–graphene

modified glassy carbon electrode. *RSC. Adv.* **2016**, 6, 90480-90488.

[25] Simioni, N. B.; Silva, T. A.; Oliveira, G. G.; et al. A nanodiamond-based electrochemical sensor for the determination of pyrazinamide antibiotic. *Sens. Actuat. B Chem.* **2017**, 250, 315-323.

[26] El-Wekil, M. M.; Mahmoud, A. M.; Alkahtani, S. A.; et al. A facile synthesis of 3D $NiFe_2O_4$ nanospheres anchored on a novel ionic liquid modified reduced graphene oxide for electrochemical sensing of ledipasvir: Application to human pharmacokinetic study. *Biosens. Bioelectron.* **2018**, 109, 164-170.

[27] Bouatra, S.; Aziat, F.; Mandal, R.; et al. The human urine metabolome. *PLoS One* **2013**, 8, e73076.

[28] Sarigul, N.; Korkmaz, F.; Kurultak, I. A new artificial urine protocol to better imitate human urine. *Sci. Rep.* **2019**, 9, 20159.

[29] Watanabe, T.; Yoshioka, S.; Yamamoto, T.; et al. The local structure in heavily boron-doped diamond and the effect this has on its electrochemical properties. *Carbon* **2018**, 137, 333-342.

[30] Xu, J.; Natsui, K.; Naoi, S.; et al. Effect of doping level on the electrochemical reduction of CO_2 on boron-doped diamond electrodes. *Diam. Relat. Mater.* **2018**, 86, 167-172.

[31] Ishii, K.; Ogata, G.; Einaga, Y. Electrochemical detection of triamterene in human urine using boron-doped diamond electrodes. *Biosens. Bioelectron.* **2022**, 217, 114666.

[32] Validation of analytical procedures: Text and methodology Q2(R1). https://database.ich.org/sites/default/files/Q2%28R1%29%20Guideline.pdf (accessed 2023-07-21).

[33] Zhang, Z.; Ogata, G.; Asai, K.; et al. Electrochemical diagnosis of urinary tract infection using boron-doped diamond electrodes. *ACS Sens* **2023**, 8, 4245-4252.

[34] Ogata, G.; Ishii, Y.; Asai, K.; et al. A microsensing system for the in

vivo real-time detection of local drug kinetics. *Nat. Biomed. Eng.* **2017**, 1, 654-666.

[35] B. Oliveira, S. C.; Oliveira-Brett, A. M. Voltammetric and electrochemical impedance spectroscopy characterization of a cathodic and anodic pre-treated boron doped diamond electrode. *Electrochim. Acta* **2010**, 55, 4599-4605.

[36] Suffredini, H. B.; Pedrosa, V. A.; Codognoto, L.; et al. Enhanced electrochemical response of boron-doped diamond electrodes brought on by a cathodic surface pre-treatment. *Electrochim. Acta* **2004**, 49, 4021-4026.

[37] Živcová, Z. V.; Petrák, V.; Frank, O.; et al. Electrochemical impedance spectroscopy of polycrystalline boron doped diamond layers with hydrogen and oxygen terminated surface. *Diam. Relat. Mater.* **2015**, 55, 70-76.

[38] Kuang, P.; Natsui, K.; Feng, C.; et al. Electrochemical reduction of nitrate on boron-doped diamond electrodes: Effects of surface termination and boron-doping level. *Chemosphere* **2020**, 251, 126364.

[39] Spãtaru, N.; Rao, T. N.; Tryk, D. A.; et al. Determination of nitrite and nitrogen oxides by anodic voltammetry at conductive diamond electrodes. *J. Electrochem. Soc.* **2001**, 148, E112-E117.

[40] Xu, X.; Liu, C.; Jia, J.; et al. A simple and inexpensive method for fabrication of ultramicroelectrode array and its application for the detection of dissolved oxygen. *Electroanalysis* **2008**, 20, 797-802.

[41] Read, T. L.; Cobb, S. J.; Macpherson, J. V. An sp^2 patterned boron doped diamond electrode for the simultaneous detection of dissolved oxygen and ph. *ACS Sens.* **2019**, 4, 756-763.

[42] Hanawa, A.; Ogata, G.; Sawamura, S.; et al. In vivo real-time simultaneous examination of drug kinetics at two separate locations using boron-doped diamond microelectrodes. *Anal. Chem.* **2020**, 92,

13742-13749.

[43] Bard, A. J.; Faulkner, L. R.; White, H. S. *Electrochemical methods: Fundamentals and applications*; John Wiley & Sons, 2001.

[44] Unic, A.; Nikolac Gabaj, N.; Miler, M.; et al. Ascorbic acid-a black hole of urine chemistry screening. *J. Clin. Lab. Anal.* **2018**, 32, e22390.

[45] Mundt, L. A.; Shanahan, K. *Graff's textbook of routine of urinalysis and body fluids (second edition)*; Lippincott Williams & Wilkins, 2011.

[46] Cougnon, C.; Gohier, F.; Belanger, D.; et al. In situ formation of diazonium salts from nitro precursors for scanning electrochemical microscopy patterning of surfaces. *Angew. Chem. Int. Ed.* **2009**, 48, 4006-4008.

[47] Edward R. Atkinson, H. H. W., Paul I. Abell and Richard E. Wing. A polarographic examination of diazotized amines. *J. Am. Chem. Soc.* **1950**, 72, 915-918.

Chapter 3 Indirect Electrochemical Detection of Creatinine in Human Urine Samples Using a Bare BDD Electrode

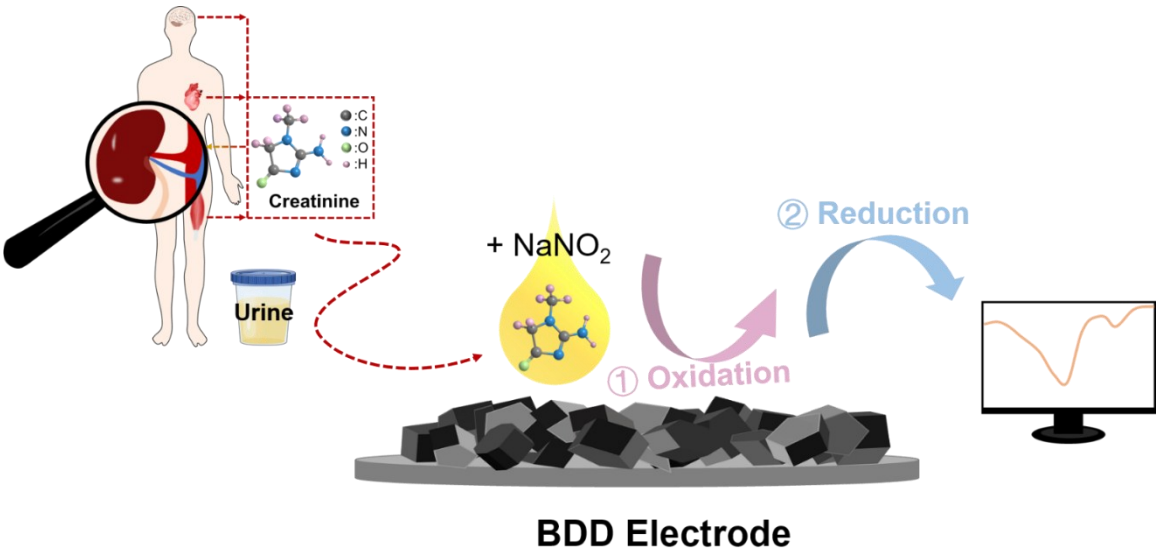

3.1 Introduction

Creatinine (CRE) is a metabolite from creatine and phosphocreatine produced during energy consumption in the muscle and tissue, which is filtered by kidneys from blood into urine [1, 2]. The CRE level in biological fluids, such as serum, urine, is a significant indicator of the body's renal functions and is vital in evaluating the body's hydration level, thyroidal malfunction and muscular disorders [3, 4]. Therefore, monitoring CRE levels in biofluids could provide crucial insights into those physiological processes, supporting the health management in long-term POCT and realising early diagnosis of acute diseases.

Traditional analysis of CRE in laboratories relies on the colourimetric Jaffé method [5], which is based on the chromogen with a characteristic orange-red colour generated from the reaction of alkaline picric acid with CRE. However, the low specificity [6], owing to the interference of numerous metabolites and drugs found in biological fluids such as glucose, ascorbic acid and cephalosporins [7], restricted the clinical application of this method. Moreover, factors like pH and temperature can affect the method's sensitivity [8], so it is necessary to provide more robust approaches to overcome these problems. Although enzymatic methods have significantly improved the detection specificity, maintaining enzyme stability requires strict conditions, which increases cost [9]. Commercial CRE test strips are available for quick POCT but are limited by inaccurate colour recognition and no quantitative results. Consequently, a simple, low-cost, sensitive and easy-to-operate analytical method is still required to quantify CRE for POCT effectively.

The electrochemical method, featured with sensitivity, rapid analysis capabilities, affordability, and ease of operation [10], has emerged as a promising alternative for CRE determination. These attributes pose

electrochemical detection as a viable technology to advance point-of-care diagnostics, addressing current limitations and enhancing healthcare accessibility.

One popular method for CRE electrochemical detection is based on the interaction of the analyte of CRE with metallic centres, such as copper [6, 9, 11, 12], silver [13], iron [14, 15] and others. Commercial electrodes, such as Pt, glassy carbon, carbon plate, and screen-printed carbon electrodes, are coated or combined with films or composites containing these metallic centres to realise CRE detection. Additionally, molecularly imprinted polymers coated electrodes [16, 17] and enzymatic sensors [18] are employed for selective detection of CRE. Bare electrodes are rarely used for CRE determination for lack of electroactivity [13, 19, 20]. While, these modifications increase sensitivity, but they require complicated electrode fabrication processes. For the realization of discrimination of compositions in complex biofluids, such as sweat, urine, and serum, a clean electrode is always required. Frequent cleaning of electrode contaminants is necessary, leading to increased difficulty and extra expenses for analysis.

Compared to blood, urine collection, handling, and disposal are simpler and more accessible [21, 22]. It is easier to facilitate long-term and frequent POCT for health management without disturbing patient integrity in contrast to repeated needle-taking in blood collection. Clinically, CRE-relevant analysis has been established as a crucial diagnostic biotic index [23]. Creatinine is an indicator of urine dilution which is used in sports competitions for the testing of stimulants and illegal drugs [19, 24]. The 24-hour urinary CRE clearance plays a key role in evaluating glomerular filtration rate and assessing renal functions in routine clinical practice [25], and is regarded as the most popular and available approach for optimizing therapy in certain empirical diseases

[26-28]. In some research, it also could be used as a marker of muscle wasting in patients with heart failure [29]. However, urine contains a complex mixture of nearly three thousand compounds [30], which presents challenges for the electrochemical detection of CRE in urine across various applications.

In this work, CRE was simply detected on a BDD electrode without any modification in an indirect electrochemical redox process by reacting with $NaNO_2$ and Cl^-. The method involved an oxidation step using chronoamperometry (CA) followed by a reduction step using differential pulse voltammetry (DPV). Initially, CRE concentrations in the range of 0−2500 mg/L (0−22 mM) were measured in Dulbecco's phosphate-buffered saline (D-PBS) and simulated urine added with 300 or 600 mg/L $NaNO_2$. Subsequently, 0−25 mg/L (0−0.22 mM) CRE in D-PBS were measured with a similar process with added 30 mg/L $NaNO_2$, and a calibration curve of CRE concentration and current response at −0.15 V (vs. Ag/AgCl) was established. This calibration curve was then used to calculate CRE concentrations in 100-fold diluted urine samples. The accuracy of this method was validated against the standard spectrophotometric method based on Jaffé's reaction. Finally, interference studies were conducted to assess the method's robustness in the presence of urea, ascorbic acid, uric acid and glucose which are common urinary substances.

3.2 Experimental

3.2.1 Chemicals and Materials

All chemical reagents were used directly without further purification. Diamond powder (~1μm) was obtained from Kemet Japan Co., Ltd. (Japan). Trimethyl borate (TMB) was purchased from Tokyo Chemical

Industry Co., Ltd (Japan). Acetone was supplied by Kanto Chemical Co., Inc (Japan). Dulbecco's phosphate buffered saline (D-PBS), H_2SO_4 (0.1 M), HCl (35%~37%), NaCl, KCl, Na_2HPO_4, $NaH_2PO_4 \cdot 2H_2O$, uric acid, Na_2SO_4, $MgSO_4 \cdot 7H_2O$, urea, NH_4Cl, $CaCl_2 \cdot 2H_2O$, trisodium citrate, NaOH, $NaNO_2$, creatinine, picric acid, ascorbic acid, agar, and D (+)-glucose were purchased from Wako Pure Chemical Industries, Ltd. (Japan). All the solutions were prepared with PB, D-PBS (using HCl change pH to 6.4) and ultrapure water (resistivity of 18.2 MΩ cm at 25 °C) which was obtained from a water purification system (Direct-Q3 UV, Merck Millipore Corp., Germany). All the urine samples were purchased from Lee BioSolutions, Inc. (USA) and Medix Biochemica Inc. (USA), and stored at −30 ºC. Two pooled urine (PU1, PU2) and six individual urines (IU1−6) were involved in the experiments. The pH of each urine sample was detected by a water quality meter (LAQUA, F-74, HORIBA Advanced Techno, Co., Ltd., Japan) and is presented in Table 3.1. Before use, these urine samples were thawed to room temperature (25 ºC) and were filtered by disposable filter units (Thermo Fisher Scientific Inc., USA) with a polyether sulfone microporous membrane (pore size: 0.45 μm) to remove precipitated protein and bacteria. The urine samples were diluted with D-PBS (pH = 6.4) at 1:100 ratio and CRE concentrations in the urine were conducted by the electrochemical test with added $NaNO_2$. Fresh CRE solutions (5, 10, 15, 20, 25,100, 500, 1000, 2000, 2500 mg/L) in D-PBS were prepared on the day of the lab. The stock $NaNO_2$ solution (30, 300 g/L) was frozen at −30 °C until use. Before electrochemical measurements, the stock $NaNO_2$ was thawed to room temperature, and 1 or 2 μL $NaNO_2$ solution was added into 1 mL fresh CRE solution, simulated urine, and diluted human urine.

Table 3.1. Information of urine samples.

Urine samples	Donors	Gender	Age	pH
PU1	≥ 3 donors	——	——	6.511
PU2	5 donors	——	——	7.127
IU1	1	Male	39	7.253
IU2	1	Male	68	5.626
IU3	1	Male	65	7.443
IU4	1	Female	30	7.018
IU5	1	Male	23	5.970
IU6	1	Male	36	6.441

3.2.2 Preparation of the BDD Electrode

The fabrication of the BDD electrode followed our group's previous works [31, 32] and is the same as that in 2.2.2.

3.2.3 Electrochemical Analysis

Electrochemical measurements of samples were conducted using a three-electrode system with an ALS CH Instruments Electrochemical Analyzer (Model 852Cs, CH Instruments Corp., USA). Two 1% BDD plates were used as working (0.363 cm^2) and counter electrodes (0.363 cm^2), and a saturated Ag/AgCl electrode (3 M KCl, Agar) was used as the reference electrode. Before electrochemical measurements, the BDD and cell were cleaned in ultrapure water using an ultrasonic cleaner for 5 min, three times. Additionally, the BDD electrode surface was cleaned using a cyclic voltammetry (CV) protocol in 0.1 M H_2SO_4, ranging from −3.0 to +3.0 V (vs. Ag/AgCl) with 40 cycles at 1 V/s using another potentiostat

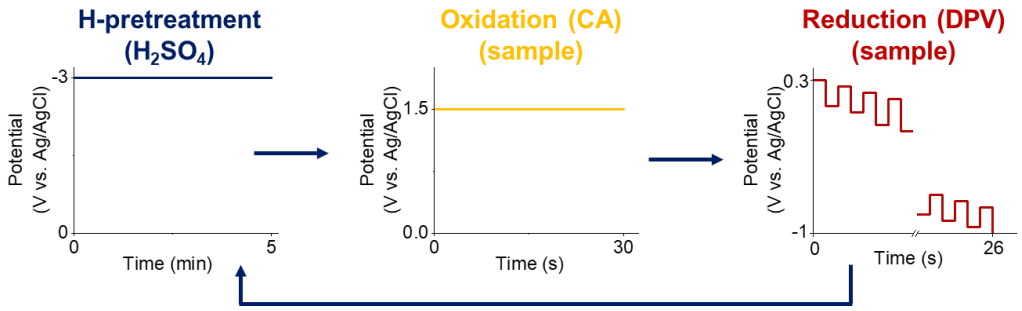

Scheme 3.1 Electrochemical procedure of detection

(Versa STAT4, AMETEK, Inc. USA). Before each sample detection, cathodic reduction by chronoamperometry (CA) in a 0.1 M H_2SO_4 aqueous solution at −3.0 V (vs. Ag/AgCl) for 5 min was processed on the BDD electrode to obtain the H-termination surface. Then, the subsequent electrochemical protocol for samples detection involved oxidation by CA at +1.5 V (vs. Ag/AgCl) for 30 s, followed by reduction using differential pulse voltammetry (DPV) with potential range from 0.3 to −1.0 V; increment of 0.005 V; amplitude of 0.4 V; pulse width of 0.05 s; pulse period of 0.1 s. The electrochemical protocol of samples measurements is shown in Scheme 3.1.

3.2.4 Spectrophotometric Analysis

In the Jaffé reaction approach, CRE was determined using a UV-Vis spectrophotometer (V-560, JASCO Corp., Japan). The quartz cuvette with an optical path length of 10 mm is used. 10 mM picric acid in a strongly basic media (250 mM NaOH) was totally mixed and reacted with 0−25 mg/L CRE (standard) or 100-fold diluted urine (H_2O, samples) for 60 min in dark, and measured by the spectrophotometer. The calibration curve between CRE concentration and absorbance at 520 nm from the standard was used to calculate the CRE in urine samples.

3.2.5 Simulated Urine

The list of components and concentrations of simulated urine with different CRE is shown in Tabel 3.2 [30]. NaOH was used to change the pH from 5.9 to 6.4. The final pH of simulated urine 1 and 2 are 5.934 and 6.452, respectively, which are in the physiological range of healthy people's urine matrix.

Table 3.2 Composition of simulated urine.

Chemical	Concentration (g/L)	
	simulated urine 1	simulated urine 2
Urea	15.00	15.00
Uric Acid	0.2500	0.2500
Trisodium Citrate	0.6320	0.6320
NaCl	1.756	1.756
KCl	2.308	2.308
NH_4Cl	1.266	1.266
$CaCl_2 \cdot 2H_2O$	0.2450	0.2450
$MgSO_4.7H_2O$	1.082	1.082
Na_2SO_4	1.700	1.700
$NaH_2PO_4.2H_2O$	2.912	2.912
Na_2HPO_4	0.6630	0.6630
Creatinine	0.1000~2.500	0.1000 ~ 2.500
NaOH	------	~ 0.0270

3.2.6 Data Analysis

Origin and Excel were used to analyse the obtained data from UV-Vis spectra and electrochemical measurements. The CRE limit of detection (LOD) value in D-PBS is calculated and described in the following equation (2)

$$LOD = 3\ SD / |\ Slope\ | \quad (2)$$

SD is the standard deviation of the current at −0.15 V of the blank. The slope is obtained from the calibration curve in Figure 3.9 C.

3.3 Results and Discussion

3.3.1 Electrochemical Measurement of CRE in D-PBS

Due to the CRE is not electroactive [19, 20], no direct oxidation or reduction response could be observed on the bare electrode [13]. Indirect determination of CRE is necessary. It was found that urinary CRE would be involved in the reaction for $NaNO_2$ detection under continuous electrochemical oxidation and reduction approach [33]. Therefore, $NaNO_2$ was added for CRE indirect determination in a similar electrochemical redox approach.

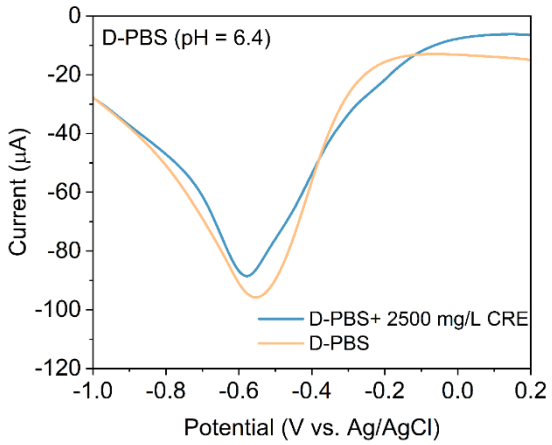

Figure 3.1. Electrochemical performance of CRE in D-PBS. DPV measurements of 0 and 2500 mg/L CRE without $NaNO_2$ in D-PBS (pH = 6.4) at the BDD electrode.

Firstly, the detection of CRE was conducted without $NaNO_2$ in D-PBS using a bare BDD electrode. As illustrated in Figure 3.1, after being electrochemically oxidised at 1.5 V (vs. Ag/AgCl) for 30 s, the DPV performance only exhibited a well-defined reduction peak at around

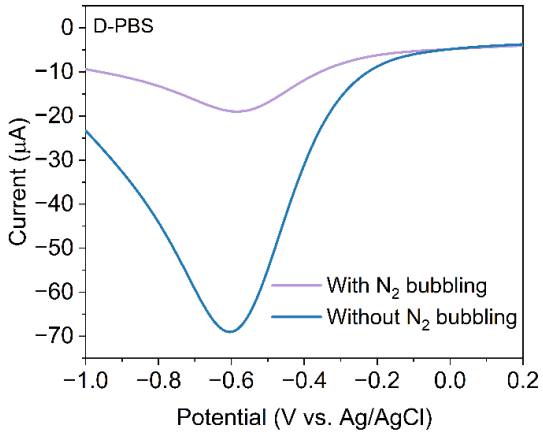

Figure 3.2. N_2 bubbling effect of D-PBS. DPV measurements of D-PBS (pH=7.4) before (blue) and after (purple) N_2 bubbling for 15 min.

−0.6 V (vs. Ag/AgCl), which is mainly attributed to the reduction of dissolved oxygen, not CRE, supporting by the noticeable decrease after 15 min N_2 bubbling in D-PBS (Figure 3.2). No reduction peak was found with CRE addition (Figure 3.1, 0 and 2500 mg/L), highlighting the difficulty of directly detecting CRE on a bare BDD electrode.

The determination of 0−2500 mg/L CRE was performed in D-PBS

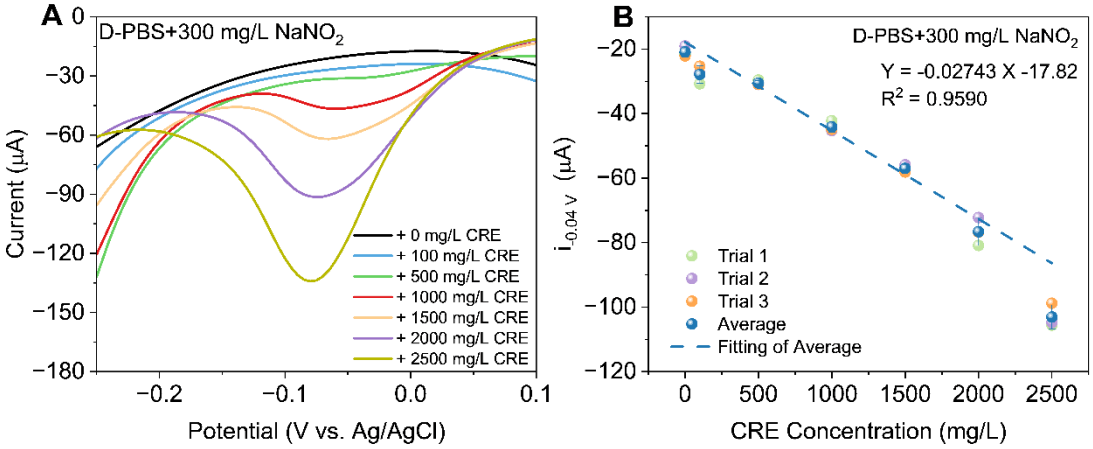

Figure 3.3. Electrochemical performance of CRE in D-PBS. A, DPV measurements of 0−2500 mg/L CRE with 300 mg/L in D-PBS (pH = 6.4) at a BDD electrode; **B**, Calibration plot of DPV reduction current at −0.04 V (vs. Ag/AgCl) and CRE concentrations.

with added 300 mg/L $NaNO_2$ on a bare BDD electrode (Figure 3.3). As shown in Figure 3.3 A, after being oxidised at 1.5 V (vs. Ag/AgCl) for 30 seconds, the DPV reduction current in the range of 0.1 to −0.25 V (vs. Ag/AgCl) exhibited a typical reduction peak at around −0.04 V (vs. Ag/AgCl), which decreased regularly as CRE concentrations increasing in D-PBS, differing significantly from the results obtained from CRE without $NaNO_2$ (Figure 3.1). Although no apparent reduction peak was observed for the low concentration range (0−100 mg/L), a noticeable current decrease compared to the blank could be found (Figure 3.3 A) When the concentration of CRE increased to 500 mg/L, a broad and shallow peak gradually emerged at around −0.04 V (vs. Ag/AgCl), becoming more characteristic with higher concentrations. This peak shifted from −0.04 V to −0.08 V (vs. Ag/AgCl) due to the "disruption of diffusion" caused by the concentration increase. Given the difficulty in identifying the peak position at a low concentration of CRE, a calibration curve between reduction current values at −0.04 V (vs. Ag/AgCl) and

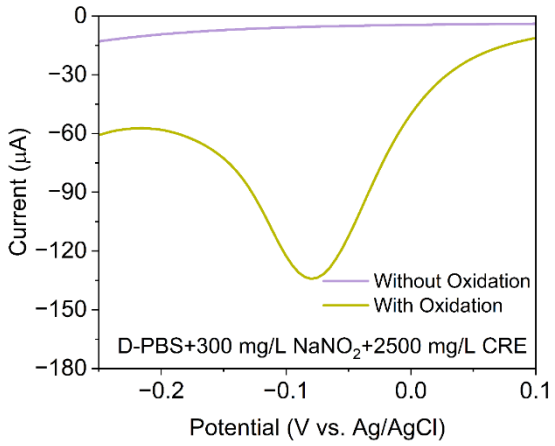

Figure 3.4. DPV measurements of CRE under different electrochemical procedures. Differential pulse voltammograms of 2500 mg/L CRE with 300 mg/L $NaNO_2$ in D-PBS (pH= 6.4) at the BDD electrode with (yellow) and without (purple) CA oxidation before DPV measurement.

CRE concentration was successfully established (Figure 3.3 B) with a coefficient of determination (R^2) as 0.9590. These results extremely demonstrate the feasibility of CRE determination on a bare BDD electrode by this method.

The successful electrochemical detection of CRE in D-PBS may be ascribed to the electrochemical redox reaction among CRE, Cl^- and $NaNO_2$ (Scheme 2.3). Unless the existence of an oxidation process, a reduction peak could not be observed in D-PBS (Figure 3.4), indicating the indirect determination of CRE. Consequently, the electrochemical strategy of utilizing oxidation followed by reduction is necessary. In the initial electrochemical step, the mixture was oxidised at 1.5 V (vs. Ag/AgCl) for 30 s, in which diazonium reaction would progress among $NaNO_2$, Cl^- and CRE under the proton surrounding generated from water oxidation (Reaction (i) in Scheme 2.3). In the next step, the generated diazonium salt would be reduced quickly, contributing to the reduction peak at around −0.04 V (vs. Ag/AgCl) [34-37]. It should be noted that no

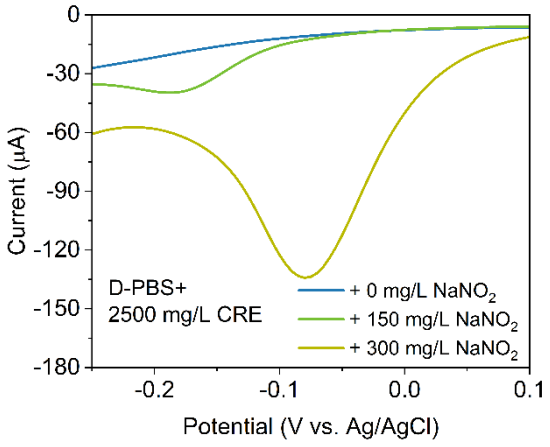

Figure 3.5. Electrochemical performances of CRE with spiked $NaNO_2$. DPV measurements of 2500 mg/L CRE with 0 (blue), 150 (green) and 300 (yellow) mg/L $NaNO_2$ in D-PBS (pH= 6.4) at the BDD electrode.

visible reduction peak at around −0.04 V (vs. Ag/AgCl) could be observed in DPV of CRE in D-PBS without $NaNO_2$ (Figure 3.5, blue line) and PB (Figure 3.6, dark blue line) without Cl^-, indicating $NaNO_2$ and Cl^- are vital in the indirect determination of CRE.

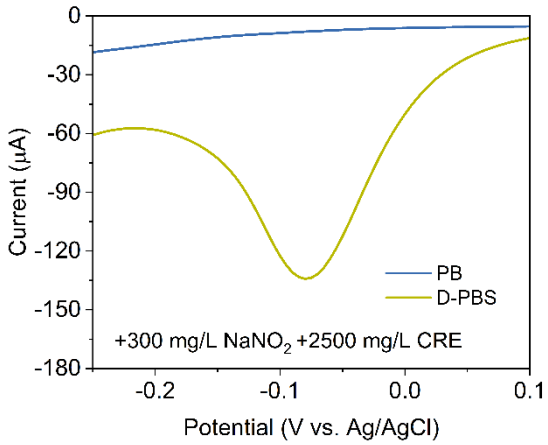

Figure 3.6. Electrochemical performances of CRE in D-PBS and PB. DPV measurements of 2500 mg/L CRE with 300 mg/L $NaNO_2$ in D-PBS (pH= 6.4, yellow) and PB (pH= 6.4, dark blue) at the BDD electrode.

3.3.2 Electrochemical Measurement of CRE in Simulated Urine

The determination of CRE in simulated urine was conducted to evaluate the feasibility of CRE determination in urine samples. Various cations (K^+, Na^+, $NH4^+$, Mg^{2+}, Ca^{2+}), anions (Cl^-, SO_4^{2-}, $H_2PO_4^-$, HPO_4^{2-}), and some organic compounds such as uric acid, urea, and trisodium citrate, which are co-existed in human urine, were used to create a basic composition for simulated urine. CRE determination in simulated urine 1 was conducted using the same procedure as that in D-PBS. As shown in Figure 3.7 A, a characteristic reduction peak at around −0.04 V (vs. Ag/AgCl) was observed. With the increase of CRE concentration from 500 to 2000 mg/L, the peak potentials shifted negatively, and apparent variations on reduction currents were observed.

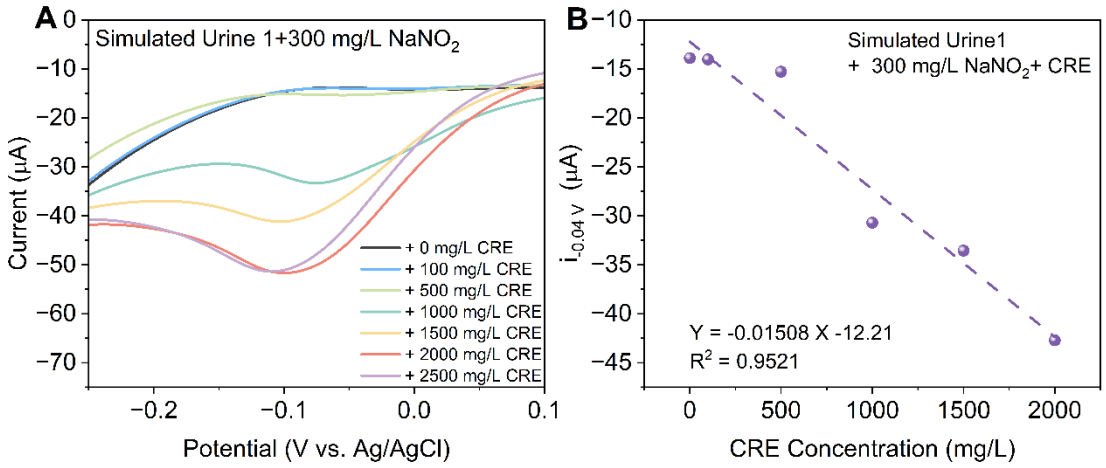

Figure 3.7. High concentrations CRE detection in simulated urine 1. **A**, DPV measurements of 0−2500 mg/L CRE with 300 mg/L $NaNO_2$ in simulate urine 1 at the BDD electrode; **B**, Calibration plot of DPV reduction current at −0.04 V (vs. Ag/AgCl) and CRE concentration (0-2000 mg/L).

Similar results were also obtained in D-PBS (Figure 3.3A). However, it is challenging to distinguish low-concentration CRE from 0 to 100 mg/L and high-concentration CRE from 2000 to 2500 mg/L by the same approach. Moreover, the reduction currents were smaller than those with the same CRE level in D-PBS, indicating some components in simulated urine would suppress the reduction response of diazonium salt mentioned in Scheme 2.3. The concentration dependence between CRE concentrations (0−2000 mg/L) and the reduction current at −0.04 V was established with a R^2 value of 0.9521 (Figure 3.7 B). The slope and intercept values of the calibration curve in simulated urine 1 were smaller than that in D-PBS (Figure 3.3 B), indicating the matrix effect of rotational (different slope) and translational (different intercept) effect in simulated urine [38], which is deserving careful consideration when determining CRE in real urine samples.

The reduction response of 0−100 mg/L, and 2000−2500 mg/L CRE at around −0.04 V (vs. Ag/AgCl) could be distinguished from each other with the addition of 600 mg/L $NaNO_2$ (Figure 3.8 A). This indicates that

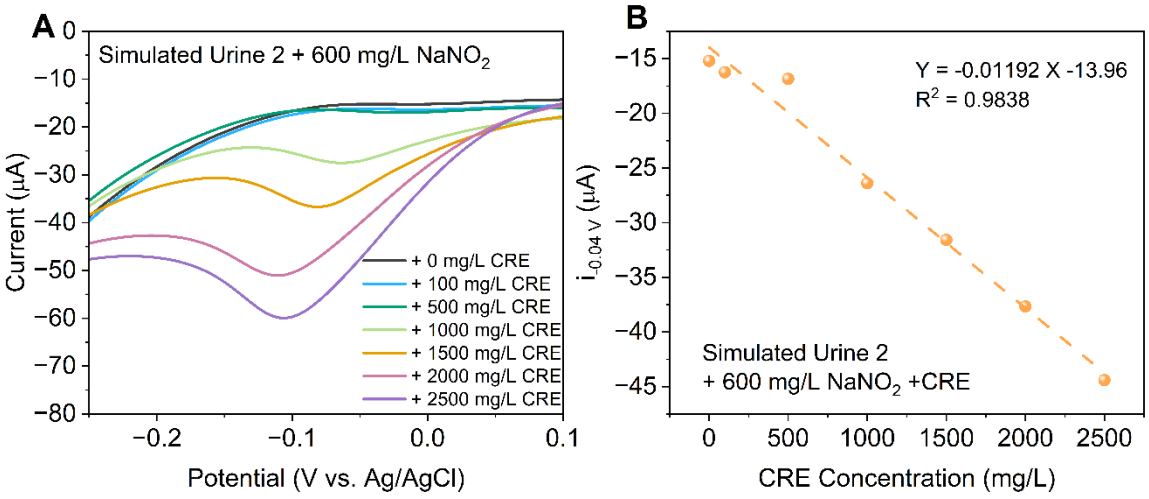

Figure 3.8. High concentrations CRE determination in simulated urine 2. A, DPV measurements of 0−2500 mg/L CRE with 600 mg/L $NaNO_2$ in simulate urine 2 using a BDD electrode; **B,** Calibration plot of reduction current at −0.04 V (vs. Ag/AgCl) and CRE concentration.

the appropriate $NaNO_2$ would be helpful for the detection of CRE in simulated urine with multiple components. A corresponding calibration plot with a R^2 value of 0.9838 (Figure 3.8 B) was obtained based on CRE concentrations and the reduction current at −0.04 V (vs. Ag/AgCl). This linearity illustrates that it is possible to discriminate and quantify CRE in the complex biofluids on a bare BDD electrode with a simple electrochemical redox process. However, the slope and intercept are still smaller than that in D-PBS (Figure 3.3 B), which indicates the matrix effect still exists and cannot be eliminated by the addition of more $NaNO_2$. This suggests an efficient method is necessary for CRE determination in complex substances, especially urine samples with large individual differences.

3.3.3 CRE Determination in Real Urine

Based on the results of CRE detection in D-PBS and simulated urine,

compared with complex electrode modification to enhance the selectivity, sensitivity and other methods such as standard addition, and dilution of complex urine samples is the preferred and simple method to overcome the matrix effect, no matter rotational and translational effect [38]. In application, dilution is easy to be accomplished by simple techniques or tools without specific training. For electrochemical detection, the lower concentration caused by dilution also requires higher sensitivity of the electrode. Comparing other bare electrodes, BDD electrodes can provide a lower detection range for many substances' determination [31, 33, 39-41].

In the determination of urinary CRE, urine samples were diluted 100-fold with D-PBS (pH = 6.4). Correspondingly, 0−25 mg/L (1%) CRE need to be tested first. Considering that an appropriate amount of $NaNO_2$ would be helpful for CRE detection, 30 mg/L $NaNO_2$ was added into D-PBS for 0−25 mg/L CRE determination using the same electrochemical redox protocol.

Figure 3.9 presents the detection of 0−25 mg/L CRE in D-PBS. Two reduction peaks at −0.5 V and −0.15 V (vs. Ag/AgCl) are evident in Figure 3.9 A. The left and typical reduction peak is due to the reduction of dissolved oxygen and is irrelative to CRE concentration. Another

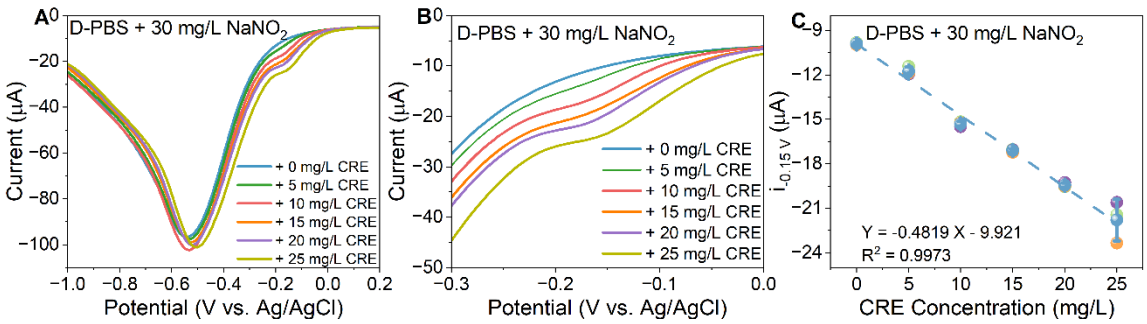

Figure 3.9. Low concentrations CRE detection in D-PBS. A, DPV measurements of 0−25 mg/L CRE with 30 mg/L $NaNO_2$ in D-PBS (pH = 6.4) using a BDD electrode; **B**, Enlarge version of DPV in area of −0.3 to 0 V (vs. Ag/AgCl); C, Calibration plot of DPV reduction current at −0.15 V (vs. Ag/AgCl) and CRE concentrations.

shallower and broader reduction peak at around −0.15 V (vs. Ag/AgCl) was found, which was likely due to the limited CRE concentrations. This peak was more negative compared to that of 0−2500 mg/L CRE in D-PBS, possibly due to the difference in the $NaNO_2$ amounts (Figure 3.5). A linear relationship between CRE concentrations and DPV reduction currents at −0.15 V (vs. Ag/AgCl) was established (Figure 3.9 C) with a R^2 of 0.9973 and a LOD of 0.3766 mg/L (3.3 μM), which is lower than the urinary CRE level in healthy people (4.4−18 mM) [3]. This also illustrates the high sensitivity of bare BDD electrodes for CRE determination using this method.

Two pooled urine and six individual urine samples were involved in the following experiments. These samples were diluted 100-fold with D-PBS, and 30 mg/L $NaNO_2$ was added to the diluted urine samples for measurements. The same electrochemical redox procedure was then applied. As shown in Figure 3.10 A, only a characteristic reduction peak

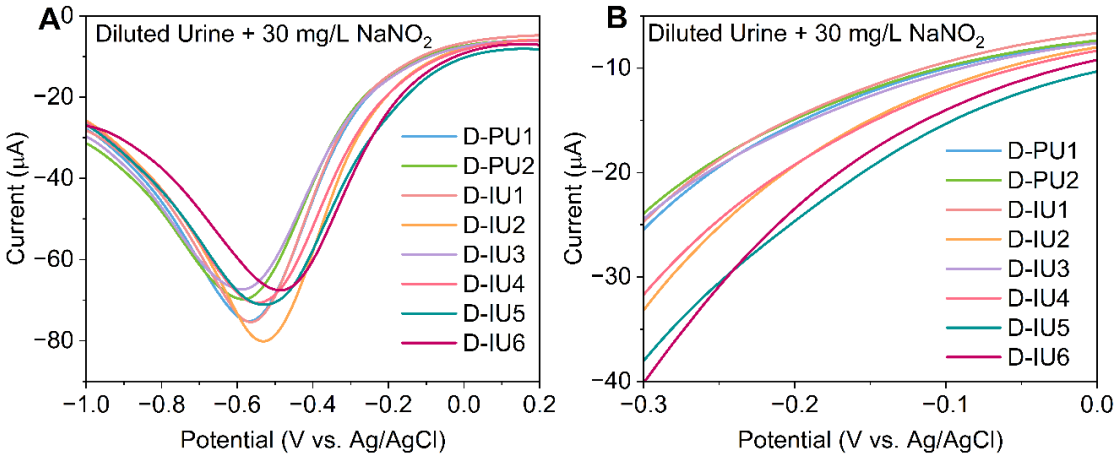

Figure 3.10. Electrochemical determination of CRE in different diluted urine samples. A, DPV measurements of 100-fold diluted pooled urine 1−2 (D-PU1 D-PU2), and diluted individual urine 1−6 (D-IU1, D-IU2, D-IU3, D-IU4, D-IU5, D-IU6) with spiked 30 mg/L $NaNO_2$; **B**, Enlarge version of DPV in area of −0.3 to 0 V (vs. Ag/AgCl).

at around −0.5 V (vs. Ag/AgCl) related to dissolved oxygen was observed, with no visible reduction peak around −0.15 V (vs. Ag/AgCl) for CRE determination, which is mainly attributed to the complex components of urine samples. Although dilution was performed, the matrix effects cannot be completely eliminated. However, it is note-worthy from Figure 3.10 B that the currents at −0.15 V (vs. Ag/AgCl) of these diluted urine samples with added $NaNO_2$ are different from each other. These inconsistencies provide the potential for CRE determination by using the reduction current here. Consequently, the CRE concentration in diluted urine were calculated using reduction currents at −0.15 V (vs. Ag/AgCl) based on the calibration curve of 0−25 mg/L CRE determination in D-PBS (Figure 3.9 C). The results are shown in Table 3.3.

Table 3.3. CRE concentrations in real urine obtained from our method and UV-Vis spectrometric method.

Samples	Calculated Concentration in Urine Samples (mg/L)	
	Electrochemical Method by BDD Sensor	UV-Vis Spectrometric Method
PU1	489.5	500.7
PU2	437.6	454.3
IU1	377.5	335.3
IU2	1042	961.7
IU3	572.5	505.4
IU4	1098	1129
IU5	1988	2136
IU6	1664	1673

The CRE concentrations in urine were confirmed by the conventional Jaffé method, and the results are shown in Figure 3.11 and Table 3.3. For this study, the same urine samples were employed in the measurements. Figure 3.12 shows the agreement between the

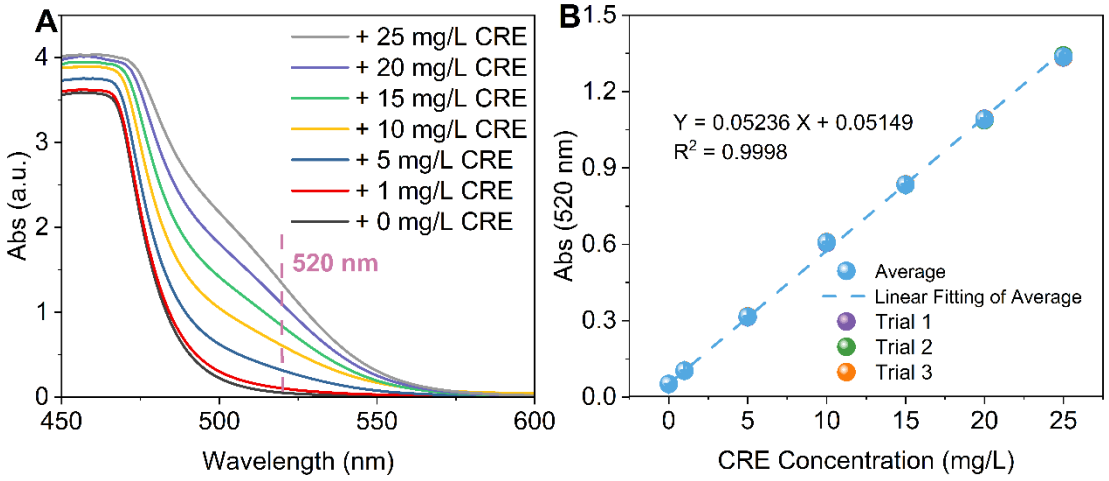

Figure 3.11. UV-Vis spectrophotometric detection of CRE. A, UV-Vis absorption spectra of 0−25 mg/L CRE with alkaline picric acid; **B**, Plot of light absorption at 520 nm and CRE concentration.

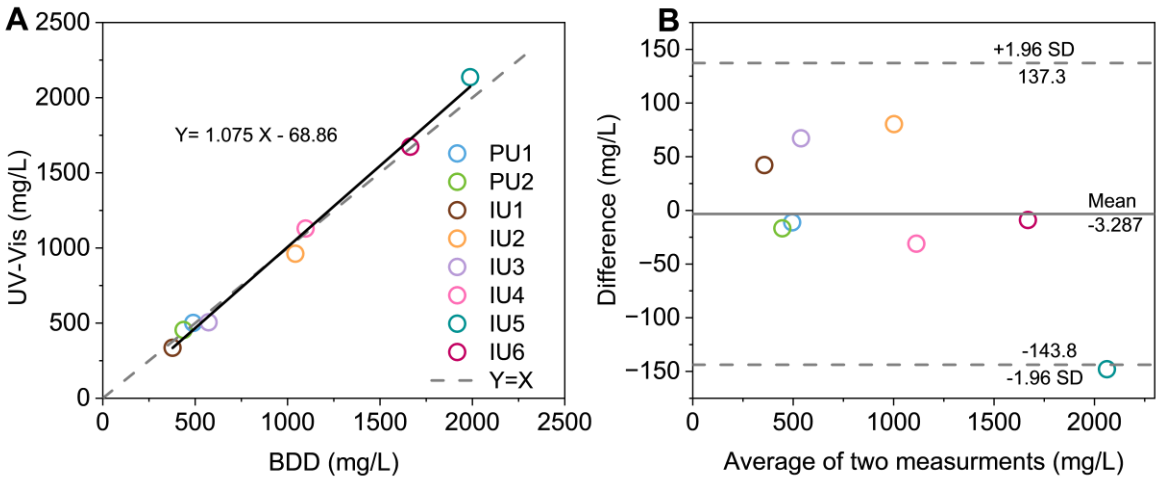

Figure 3.12. Quantification of CRE concentration in human urine. A, Comparison of the CRE concentration in the urine obtained from electrochemical and UV-Vis measurements. The solid line represents Deming regression fitted to the data (slope = 1.075, R = 0.9964) and the dashed line represents y = x equivalence. **B**, Bland–Altman analysis of the difference between the electrochemical and UV-Vis measurements (subtraction of the former from the latter) plotted as a function of the mean of these values. The solid grey line indicates the value of bias (that is, the mean difference, −3.287), whereas the dashed lines represent the 95% confidence limit (that is, the range of 1.96 SD; −143.8 to 137.3 mg/L).

electrochemical and the Jaffé method. As shown in Figure 3.12 A, the CRE concentrations determined using the bare BDD sensor were

equivalent to the results obtained from UV-Vis spectrometry, with a coefficient of correlation (R) as 0.9964. The Bland−Altman analysis (Figure 3.12 B) indicates a slight bias of −3.287 ± 71.71 mg/L (the average difference between the values obtained by two methods ± SD). Almost all data points fell within a 95% confidence interval of −143.8 to 137.3 mg/L, indicating little systematic differences between these two methods. Although the result for individual urine 5 (IU5) fells on the edge of 95% confidence interval, the coefficients of variation (CV) using UV-Vis spectra result as the mean and electrochemical calibration data (n = 3) as individual data points is 8.1 % (< 15%), which is accepted as a standard precision level for bioanalytical assays [42]. The strong agreement between these two methods indicates the feasibility of using an easy electrochemical redox approach on a bare BDD electrode for urinary CRE quantification, providing a reliable and accessible electrochemical technique for urinary CRE POCT and healthcare accessibility.

3.3.4 Interference Study and Limitation

Given the matrix effect, the influence of metabolites commonly found in urine also needs attention. Adding certain substances commonly present in urine samples to the urine can visually reveal their effects on the determination of urinary CRE. Therefore, 2500 mg/L (41.6 mM) urea, 144 mg/L (0.8 mM) glucose, 100 mg/L (0.6 mM) uric acid and 88 mg/L (0.5 mM) ascorbic acid were directly added to PU1 for measurements, and the results are shown in Figure 3.13. As observed in Figure 3.13 A, the addition of urea, glucose, and uric acid does not influence the DPV response of PU1 together with 300 mg/L $NaNO_2$. However, the current value of PU1 with the addition of ascorbic acid shows a decrease. Due to the appearance of characteristic reduction peaks at around −0.04 V (vs.

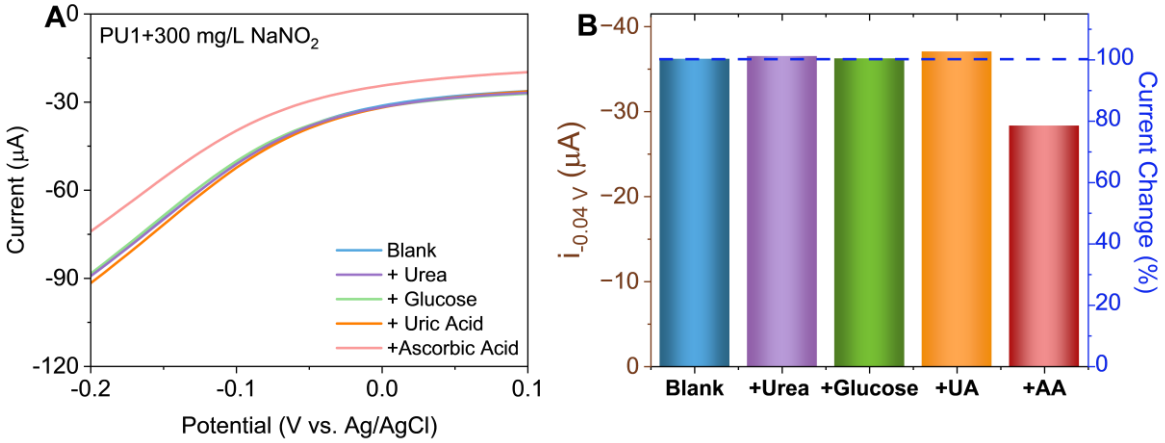

Figure 3.13. Interference study of urea, glucose, uric acid (UA), and ascorbic acid (AA) in pooled urine 1. A, The DPV reduction current of PU1 with 300 mg/L $NaNO_2$ (blank) and added with 2500 mg/L urea, 144 mg/L glucose, 100 mg/L uric acid (UA) and 88 mg/L ascorbic acid (AA); **B**, Current change at −0.04 V after added with interference.

Ag/AgCl) in the high concentrations of CRE in D-PBS and simulated urine, the reduction current here of PU1 without dilution was used to evaluate the influence of ascorbic acid. The reduction current value at −0.04 V (vs. Ag/AgCl) of the sample with added ascorbic acid shows an approximately 21.8 % decrease (Figure 3.13 B), which is non-negligible. It is recommended that people who take amounts of ascorbic acid or fruits with high Vitamin C in a short time should be cautious, as the urinary CRE amount results determined by this method may be underestimated. The limitation of this method is summarized in Table 3.4.

In addition, the urine of urinary tract infection (UTI) patients has a high potential containing $NaNO_2$. The $NaNO_2$ detection range in patients' urine is around 0.6−1 mg/L [45]. In our case, the urine samples were diluted 100 times, and 30 mg/L $NaNO_2$ was added for CRE detection. There won't be a big difference among diluted UTI patients' urine with $NaNO_2$ less than 0.03% $NaNO_2$.

Table 3.4 Summary of the limitations of different methods for CRE detection

Method	Advantages	Disadvantages	LOD (mg/L)	Ref
Colorimetry	Sensitive, easy, low-cost, rapid (15-30 min)	Low specificity, toxic and explosive chemical	4.0	[46]
HPLC	Sensitive, low detection limit	High cost, time-consuming (several hours), sample pretreatments, trained personal	0.50	[47]
Raman spectrometry	Rapid (few minutes), trace-level detection	Low specificity and sensitivity in complex biological samples	1.4	[5]
Electro-chemistry	Sensitive, fast (in 1 min), low-cost, easy, bare electrode	Interference of ascorbic acid	0.38	This work

HPLC: High-performance liquid chromatography

3.4 Conclusion

In this work, an easy, rapid, accurate and non-enzymatic electrochemical method for the indirect and determination of CRE in human urine was proposed using a BDD electrode. The electrode could be directly used without any modification. The detection is based on CRE electrochemical redox reaction with $NaNO_2$ and Cl^-. Samples were measured with a continuous redox approach with oxidation by CA at 1.5 V (vs. Ag/AgCl) followed by reduction by DPV. Linear concentration dependence was successfully established between the cathodic reduction currents of DPV measurements and CRE concentrations, with the LOD lower than the human healthy urinary CRE level. The CRE concentrations in different urine, calculated from the calibration curve built in D-PBS, exhibit good agreement with the results obtained from the standard spectrophotometric method based on the Jaffé reaction. This method could be used to quickly monitor urinary CRE concentrations,

providing insights into renal functions and human physiological processes and supporting future health management in POCT and early diagnosis of diseases. However, it is worth being cautious about the high intake of ascorbic acid or foods containing Vitamin C in a short time before detection.

3.5 Reference

[1] Guinovart, T.; Hernandez-Alonso, D.; Adriaenssens, L.; et al. Characterization of a new ionophore-based ion-selective electrode for the potentiometric determination of creatinine in urine. *Biosens. Bioelectron.* **2017**, 87, 587-592.

[2] Li, Y.; Luo, L.; Nie, M.; et al. A graphene nanoplatelet-polydopamine molecularly imprinted biosensor for ultratrace creatinine detection. *Biosens. Bioelectron.* **2022**, 216, 114638.

[3] Rakesh Kumar, R. K.; Shaikh, M. O.; Chuang, C. H. A review of recent advances in non-enzymatic electrochemical creatinine biosensing. *Anal. Chim. Acta* **2021**, 1183, 338748.

[4] Pundir, C. S.; Kumar, P.; Jaiwal, R. Biosensing methods for determination of creatinine: A review. *Biosens. Bioelectron.* **2019**, 126, 707-724.

[5] Zhu, W.; Wen, B. Y.; Jie, L. J.; et al. Rapid and low-cost quantitative detection of creatinine in human urine with a portable Raman spectrometer. *Biosens. Bioelectron.* **2020**, 154, 112067.

[6] Chen, C. H.; Lin, M. S. A novel structural specific creatinine sensing scheme for the determination of the urine creatinine. *Biosens. Bioelectron.* **2012**, 31, 90-94.

[7] Lad, U.; Khokhar, S.; Kale, G. M. Electrochemical creatinine biosensors. *Anal. Chem.* **2008**, 80, 7910–7917.

[8] Walsh, D. A.; Dempsey, E. Comparison of electrochemical, electrophoretic and spectrophotometric methods for creatinine determination in biological fluids. *Anal. Chim. Acta* **2002**, 459, 187–198.

[9] Raveendran, J.; P.E, R.; T, R.; et al. Fabrication of a disposable non-enzymatic electrochemical creatinine sensor. *Sens. Actuat. B Chem.* **2017**, 243, 589-595.

[10] Jiang, H.; Jiang, D.; Liu, X.; et al. A self-driven PET chip-based imprinted electrochemical sensor for the fast detection of *salmonella*. *Sens. Actuat. B Chem.* **2021**, 349, 130785.

[11] Pedrozo-Peñafiel, M. J.; Lópes, T.; Gutiérrez-Beleño, L. M.; et al. Voltammetric determination of creatinine using a gold electrode modified with nafion mixed with graphene quantum dots-copper. *J. Electroanal. Chem.* **2020**, 878, 114561.

[12] Boobphahom, S.; Ruecha, N.; Rodthongkum, N.; et al. A copper oxide-ionic liquid/reduced graphene oxide composite sensor enabled by digital dispensing: Non-enzymatic paper-based microfluidic determination of creatinine in human blood serum. *Anal. Chim. Acta* **2019**, 1083, 110-118.

[13] Viswanath, K. B.; Devasenathipathy, R.; Wang, S.-F.; et al. A new route for the enzymeless trace level detection of creatinine based on reduced graphene oxide/silver nanocomposite biosensor. *Electroanalysis* **2017**, 29, 559-565.

[14] Fava, E. L.; Martimiano do Prado, T.; Almeida Silva, T.; et al. New disposable electrochemical paper-based microfluidic device with multiplexed electrodes for biomarkers determination in urine sample. *Electroanalysis* **2020**, 32, 1075-1083.

[15] Sriramprabha, R.; Sekar, M.; Revathi, R.; et al. Fe_2O_3/polyaniline supramolecular nanocomposite: A receptor free sensor platform for the quantitative determination of serum creatinine. *Anal. Chim. Acta* **2020**,

1137, 103-114.

[16] Reddy, K. K.; Gobi, K. V. Artificial molecular recognition material based biosensor for creatinine by electrochemical impedance analysis. *Sens. Actuat. B Chem.* **2013**, 183, 356-363.

[17] Patel, A. K.; Sharma, P. S.; Prasad, B. B. Development of a creatinine sensor based on a molecularly imprinted polymer-modified sol-gel film on graphite electrode. *Electroanalysis* **2008**, 20, 2102-2112.

[18] Premanode, B.; Toumazou, C. A novel, low power biosensor for real time monitoring of creatinine and urea in peritoneal dialysis. *Sens. Actuat. B Chem.* **2007**, 120, 732-735.

[19] Ngamchuea, K.; Wannapaiboon, S.; Nongkhunsan, P.; et al. Structural and electrochemical analysis of copper-creatinine complexes: Application in creatinine detection. *J. Electrochem. Soc.* **2022**, 169, 020567.

[20] Bajpai, S.; Akien, G. R.; Toghill, K. E. An alkaline ferrocyanide non-enzymatic electrochemical sensor for creatinine detection. *Electrochem. Commun.* **2024**, 158, 107624.

[21] Zhang, X.; Jiang, X. Y.; Zhao, L.; et al. Urine self-sampling kit combined with an automated preparation-sampler device for convenient and reliable analysis of arsenic metabolites by HPLC-ICPMS. *Anal. Chem.* **2024**, 96, 1742-1749.

[22] Choi, J. W.; Song, Y. C.; Cheong, N. Y.; et al. Concentrations of blood and urinary arsenic species and their characteristics in general korean population. *Environ. Res.* **2022**, 214, 113846.

[23] Rocío Cánovas; María Cuartero; Crespo, G. A. Modern creatinine (bio)sensing: Challenges of point-of-care platforms. *Biosens. Bioelectron.* **2019**, 130, 110-124.

[24] Eleni I. Tzianni; Ioannis Moutsios; Dimitrios Moschovas; et al. Smartphone paired SIM card-type integrated creatinine biosensor. *Biosens. Bioelectron.* **2022**, 207, 114204.

[25] Huang, C. Y.; Guiza, F.; Wouters, P.; et al. Development and validation of the creatinine clearance predictor machine learning models in critically ill adults. *Crit. Care* **2023**, 27, 272.

[26] Carrie, C.; Rubin, S.; Sioniac, P.; et al. The kinetic glomerular filtration rate is not interchangeable with measured creatinine clearance for prediction of piperacillin underexposure in critically ill patients with augmented renal clearance. *Crit. Care* **2018**, 22, 177.

[27] Ogata, S.; Akashi, Y.; Sakusabe, T.; et al. A multiple 24-hour urine collection study indicates that kidney function decline is related to urinary sodium and potassium excretion in patients with chronic kidney disease. *Kidney Int* **2022**, 101, 164-173.

[28] Jedrusik, P.; Symonides, B.; Gaciong, Z. Performance of 24-hour urinary creatinine excretion-estimating equations in relation to measured 24-hour urinary creatinine excretion in hospitalized hypertensive patients. *Sci. Rep.* **2019**, 9, 3593.

[29] Pandhi, P.; Streng, K. W.; Anker, S. D.; et al. The value of spot urinary creatinine as a marker of muscle wasting in patients with new-onset or worsening heart failure. *J. Cachexia Sarcopenia Muscle* **2021**, 12, 555-567.

[30] Sarigul, N.; Korkmaz, F.; Kurultak, I. A new artificial urine protocol to better imitate human urine. *Sci. Rep.* **2019**, 9, 20159.

[31] Ishii, K.; Ogata, G.; Einaga, Y. Electrochemical detection of triamterene in human urine using boron-doped diamond electrodes. *Biosens. Bioelectron.* **2022**, 217, 114666.

[32] Moriyama, H.; Ogata, G.; Nashimoto, H.; et al. A rapid and simple electrochemical detection of the free drug concentration in human serum using boron-doped diamond electrodes. *Analyst* **2022**, 147, 4442-4449.

[33] Zhang, Z.; Ogata, G.; Asai, K.; et al. Electrochemical diagnosis of urinary tract infection using boron-doped diamond electrodes. *ACS Sens*

2023, 8, 4245-4252.

[34] Stève Baranton; Bélanger, D. Electrochemical derivatization of carbon surface by reduction of in situ generated diazonium cations. *J. Phys. Chem. B* **2005**, 109, 24401-24410.

[35] Cougnon, C.; Gohier, F.; Belanger, D.; et al. In situ formation of diazonium salts from nitro precursors for scanning electrochemical microscopy patterning of surfaces. *Angew. Chem. Int. Ed.* **2009**, 48, 4006-4008.

[36] Edward R. Atkinson, H. H. W., Paul I. Abell and Richard E. Wing. A polarographic examination of diazotized amines. *J. Am. Chem. Soc.* **1950**, 72, 915-918.

[37] Edward R. Atkinson; Charles E. Garland; Butler, A. F. A polarographic examination of diazotized amines. II. Additional coulometric data. *J. Am. Chem. Soc.* **1953**, 75, 983-984.

[38] Thompson, M.; Ellison, S. L. R. A review of interference effects and their correction in chemical analysis with special reference to uncertainty. *Accred. Qual. Assur.* **2004**, 10, 82-97.

[39] Hanawa, A.; Ogata, G.; Sawamura, S.; et al. In vivo real-time simultaneous examination of drug kinetics at two separate locations using boron-doped diamond microelectrodes. *Anal. Chem.* **2020**, 92, 13742-13749.

[40] Triana, Y.; Ogata, G.; Tomisaki, M.; et al. Blood oxygen sensor using a boron-doped diamond electrode. *Anal. Chem.* **2022**, 94, 3948-3955.

[41] Chiku, M.; Nakamura, J.; Fujishima, A.; et al. Conformational change detection in nonmetal proteins by direct electrochemical oxidation using diamond electrodes. *Anal. Chem.* **2008**, 80, 5783-5787.

[42] Ates, H. C.; Roberts, J. A.; Lipman, J.; et al. On-site therapeutic drug monitoring. *Trends Biotechnol.* **2020**, 38, 1262-1277.

[43] Koeijers, J. J.; Kessels, A. G.; Nys, S.; et al. Evaluation of the nitrite

and leukocyte esterase activity tests for the diagnosis of acute symptomatic urinary tract infection in men. *Clin. Infect. Dis.* **2007**, 45, 894-896.

[44] Zorc, J. J.; Kiddoo, D. A.; Shaw, K. N. Diagnosis and management of pediatric urinary tract infections. *Clin Microbiol Rev* **2005**, 18, 417-422.

[45] *Multistix ® pro 10ls reagent strips* SIEMENS Healthcare Diagnostics Inc, 2017. https://content.doclib.siemens-healthineers.com/rest/v1/view?document-id=370559 (accessed 2024-08-20).

[46] Tarim, E. A.; Tekin, H. C. Colorimetric detection of serum creatinine on a miniaturized platform using hue-saturation-value space analysis. *Sci. Rep.* **2024**, 14, 19441.

[47] Tsikas, D.; Wolf, A.; Frölich, J. r. C. Simplified HPLC method for urinary and circulating creatinine. *Clin. Chem.* **2004**, 50, 201-203.

Chapter 4 Electrochemical Detection of Edoxaban in Human Plasma Samples Using a Bare BDD Electrode

4.1 Introduction

Coagulation, or blood clotting, is a vital physiological response to internal or external injuries. However, disruptions in this process, such as hypercoagulation, can result in excessive blood clots, leading to vascular blockages and thrombosis [1, 2]. Clinically, this condition manifests primarily as myocardial infarction [3], stroke [4], or venous thromboembolism [5].

Anticoagulant medications are widely used to prevent or slow blood clot formation. They play a critical role in the prevention of thrombosis associated with atrial fibrillation [6], heart valve diseases [7], post-cardiac surgery [8], or artificial heart valve replacement. Additionally, anticoagulants are essential for preventing and treating deep vein thrombosis [9] and pulmonary embolism [10].

Since their introduction in 2010, direct oral anticoagulants (DOAC), characterized by oral administration and rapid onset of action, have largely replaced vitamin K antagonists (VKAs) in clinical practice [11]. DOACs are small molecules that inhibit clotting factor Xa or thrombin by occupying their catalytic sites, thereby preventing substrate activation [12]. This mode of action provides a broader therapeutic window, reduces the need for stringent monitoring, and lowers the risk of drug-drug interactions [9, 11].

Edoxaban (EDX) is a kind of DOACs, developed by Daiichi Sankyo (Japan) in 2011. It is a highly selective and direct inhibitor of clotting factor Xa [13, 14]. It achieves peak plasma concentration within 1–2 hours of administration and exhibits low protein binding [15]. Unlike VKAs, DOACs, such as EDX, rivaroxaban, and apixaban do not require routine laboratory monitoring of anticoagulant activity [16]. However, assessing EDX plasma levels may be necessary for specific clinical

scenarios, including trauma, urgent or emergent surgery, thrombolytic therapy for recent strokes, or in patients with unique conditions such as extreme body weight, altered renal function, gastrointestinal malabsorption, suspected drug interactions, or overdose [14]. And the concern has emerged that the measurement of drug concentration might be needed to assess proper drug concentration which would prevent increased bleeding risk, blood clot and recurrence.

Several laboratory methods have been developed to determine EDX plasma levels [17-21]. Liquid chromatography/tandem mass spectrometry (LC-MS/MS) methods have been developed to determine EDX plasma levels [15]. However, its high instrument complexity, lab-intensive procedures, and extended processing times hinder utility in emergencies and home healthcare settings [22]. Thus, alternative clinical and point-of-care testing strategies are needed to enhance anticoagulation management.

The electrochemical method features rapid, accurate, and cost-effective analysis and is a promising alternative. Nonetheless, modified electrode surfaces designed to improve sensitivity, selectivity, and stability are often complex or impractical [2]. In contrast, bare electrodes present an economical and environmentally friendly solution for EDX determination.

This study focuses on developing a simple and sensitive electrochemical method for determining EDX in plasma using a bare BDD electrode. EDX was analyzed through sequential electrochemical oxidation and reduction processes. Initially, 1000 nM EDX was detected using cyclic voltammetry (CV) across two cycles in the range of –1.0 to +1.5 V (vs. Ag/AgCl) with varying initial scan directions to validate the detection procedure. Subsequently, concentrations of 10–500 nM EDX were measured in phosphate-buffered saline (PBS) via electrochemical

oxidation using chronoamperometry (CA), followed by reduction using square wave voltammetry (SWV). A concentration-dependent relationship between the reduction current and EDX concentration was established. Finally, the same procedure was applied to detect 10–500 nM EDX spiked into plasma samples.

4.2 Experimental

4.2.1 Chemicals and Materials

All chemical reagents were used directly without further purification. Diamond powder (~1μm) was obtained from Kemet Japan Co., Ltd. (Japan). Trimethyl borate (TMB) was purchased from Tokyo Chemical Industry Co., Ltd (Japan). Acetone was supplied by Kanto Chemical Co., Inc. (Japan). Phosphate buffered saline (PBS), H_2SO_4 (1 M), NaOH, and dimethyl sulfoxide (DMSO) were purchased from FUJIFILM Wako Pure Chemical Industries, Ltd. (Japan). Edoxaban tosylate (≥98%, HPLC) was purchased from Sigma Aldrich. Co. Ltd, and was dissolved in dimethyl sulfoxide (DMSO) for long-term storage without any purification. The stock solution (10, 30, 100, 300, 500, 1000 μM) was frozen at −30 °C until use. Before use, they were thawed to room temperature, and 1 μL stock solution was added into 1 mL PBS or human plasma for the electrochemistry measurement. Pooled human plasma was purchased from COSMO Bio Co., Ltd and stored at −30 °C. Before use, it was thawed to room temperature.

4.2.2 Preparation of the BDD Electrode

The fabrication of the BDD electrode followed our group's previous works [23, 24] and is the same as that in 2.2.2.

4.2.3 Electrochemical Analysis

Electrochemical measurements of samples were conducted using a three-electrode system with an ALS CH Instruments Electrochemical Analyzer (Model 852Cs, CH Instruments Corp., USA). Two 1% BDD plates were used as working and counter electrodes (0.363 cm^2), and a saturated Ag/AgCl electrode (3 M KCl, Agar) was used as the reference electrode. Before measurements, the BDD and cell were cleaned in ultrapure water using an ultrasonic cleaner for 5 min, three times. Additionally, the BDD electrode surface was cleaned using a CV protocol in PBS, ranging from −1.5 to +1.5 V (vs. Ag/AgCl) with 40 cycles in a scan rate of 1V/s. EDX in PBS was measured using two-cycle CV measurements in the range of −1.0 to 1.5 V, with an initial potential of 0 V (vs. Ag/AgCl), the initial direction of positive and negative, respectively, and the scan rate was 0.1 V/s. Before sample detection, anodic oxidation and cathodic reduction by CA in 1M KOH aqueous solution at +3.0 V (vs. Ag/AgCl) and 0.5 M H_2SO_4 at −3.0 V (vs. Ag/AgCl) for 1 min was processed on the BDD electrode to obtain the O/H-termination surface. EDX in PBS was detected by using CV measurement in the range of −1.0 to 1.5 V, with an initial potential of 0 V (vs. Ag/AgCl), the initial direction of positive on O/H terminated BDD, and the scan rate of 0.1 V/s. Then, the subsequent electrochemical protocol for sample detection on O-terminated BDD involved oxidation by CA at +1.4 V (vs. Ag/AgCl) for 30 s, followed by reduction using square wave voltammetry (SWV) with the potential range from 0.4 to −1.0 V, increment of 0.01 V, amplitude of 0.05 V, frequent of 10 Hz. The protocol is shown in Scheme 4.1.

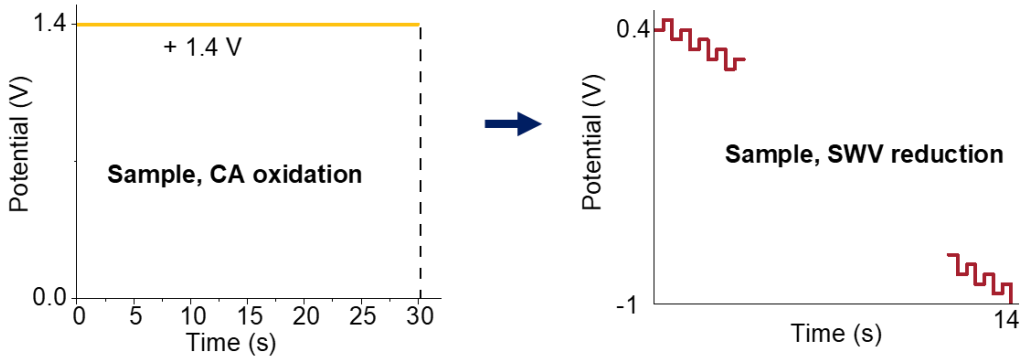

Scheme 4.1 Electrochemical procedure of detection.

4.2.4 Data Analysis

Origin and Excel were used to analyze the obtained data from electrochemical measurements. The CRE limit of detection (LOD) value in PBS is calculated and described in the following equation (3)

$$LOD = 3\ SD / | Slope | \quad (3)$$

SD is the standard deviation of the current at −0.8 V of the blank. The slope is obtained from the calibration curve in Figure 4.4 B.

4.3 Results and Discussion

4.3.1 EDX Detection in PBS

Firstly, a two-cycle CV protocol in the range of -1.0 to +1.5 V was performed in 1000 nM EDX in PBS. Figure 4.1 shows different redox states of EDX on the electrochemical reaction. In the left panels, the applied potential was scanned from 0 to -1.0 V for reducing EDX directly, and then the potential was shifted to the positive range to +1.5 V. On the contrary, in the right panels, EDX was been oxidized followed by reduction. The cyclic voltammetry analysis of EDX was carried out twice (red and blue curves). For control data, PBS alone was tested (black

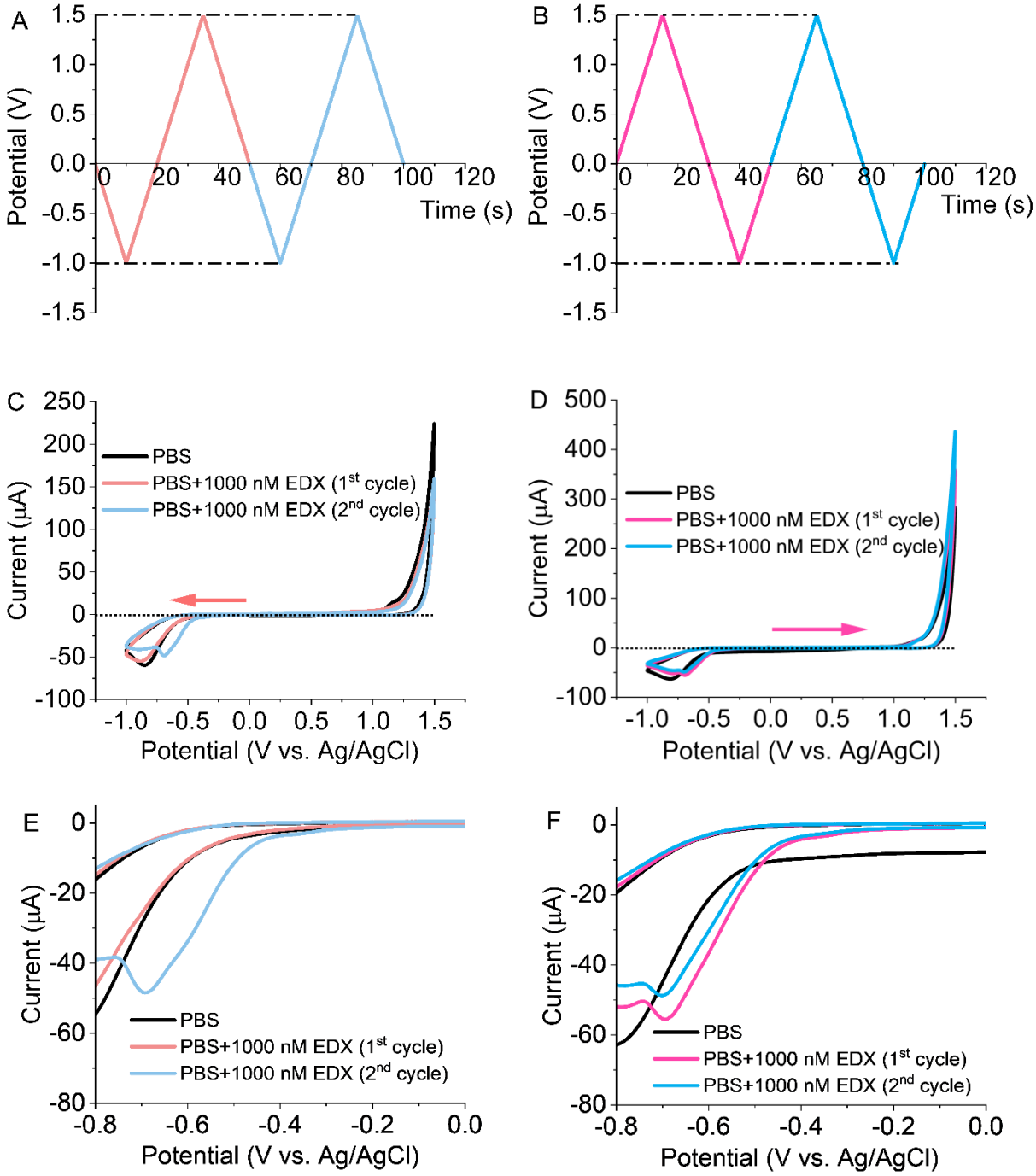

Figure 4.1 Different redox states of EDX on the electrochemical reaction. CV protocols of 1000 nM EDX in PBS on a BDD electrode with different initial scan directions: **A**, negative; **B**, positive; CV performance of 1000 nM EDX in PBS with different initial scan directions: **C**, negative; **D**, positive; **E**, **F**, enlarged version of C and D in the range of −0.8 to 0 V, respectively. Conditions: CV, potential range, −1 to +1.5 V, initial potential, 0 V; two cycles, scan rate, 0.1 V/s.

curve). CV protocols with different initial scan directions of negative and positive were shown in Figure 4.1 A and B, respectively. As shown in Figure 4.1 C and D, the CV performances of either positive or negative initial scan did not show a response in the positive range compared with PBS. However, in the negative range, a peak at around –0.69 V (vs. Ag/AgCl) could be easily observed. The difference is that in the CV with a positive initial scan, the peak would be observed in both the first and second cycles (Figure 4.1 F). Otherwise, the peak only shows in the second cycle in the CV performance with a negative initial scan (Figure 4.1 E). The results indicate that the reaction of EDX reduction requires the oxidised form of the compound.

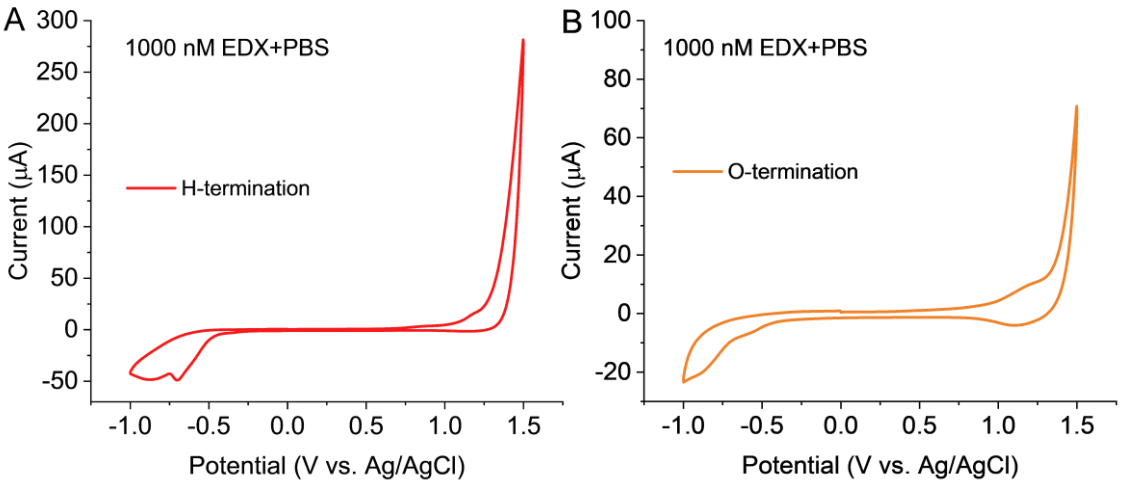

Figure 4.2 CV performance of 1000 EDX in PBS on BDD electrode with different termination. **A**, H-terminated BDD; **B**, O-terminated BDD. Conditions: CV, potential range, −1 to +1.5, initial potential, 0 V; initial scan direction, positive; one cycle, scan rate, 0.1 V/s.

Surface termination is a popular way to modify the termination bonds at BDD electrodes altering their electrochemical and physicochemical properties. Cathodic reduction and anodic oxidation are used to obtain the H- and O-termination. As shown in Figures 4.2 A and B, in the reduction range, the CV performances of EDX on H-terminated

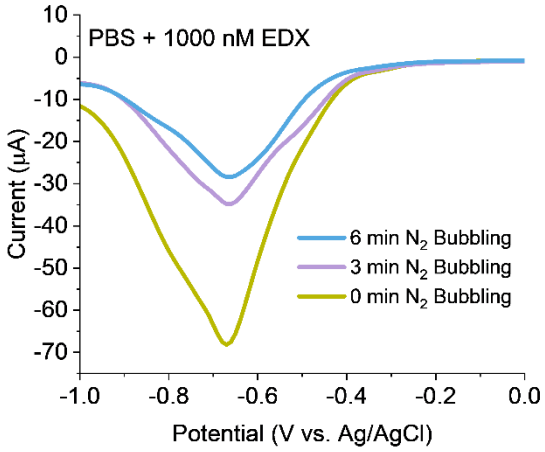

Figure 4.3 SWV performance of EDX with N_2 bubbling. SWV performance of 1000 nM EDX in PBS on a BDD electrode after 0, 3, 6 min N_2 bubbling.

BDD show higher responses than those of O-terminated BDD electrodes. Although H-terminated BDD often exhibits higher electrical conductivity, the peak here may be overlaid by the reduction of dissolved oxygen. As could be seen in Figure 4.3, the SWV of EDX showed an apparent decreased peak with N_2 bubbling. The results indicate the H-terminated BDD would be affected by the dissolved oxygen, which would increase the experiment error. O-terminated BDD was used for the following experiments to obtain a simple detection procedure for application.

SWV offers higher sensitivity and a broad dynamic range for the measurement of analysts than CV. Therefore, 0-500 nM EDX were measured by continued oxidation of CA followed by the reduction of SWV. Initially, the blank with DMSO in PBS was examined (black line). As could be seen in Figure 4.4 A, without EDX, the DMSO and PBS don't show any reduction peak in the range of −0.6 to −1.0 V (vs. Ag/AgCl). The reduction currents value at around −0.8 V (vs. Ag/AgCl) increased as the EDX concentration increased from 10 to 500 nM. Until the EDX concentration increases to 100 nM, a reduction peak around here gradually becomes obvious. A calibration curve was obtained between the

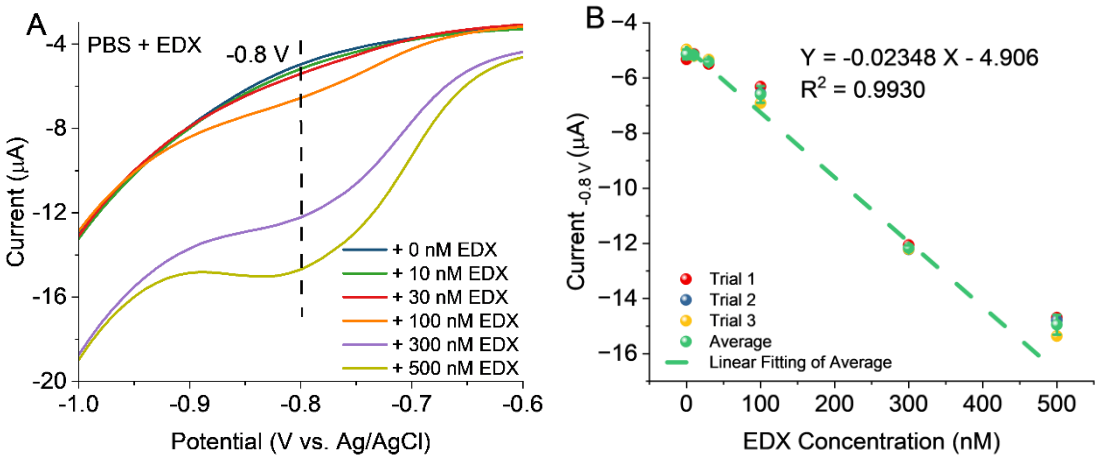

Figure 4.4 EDX detection in PBS. A, SWV performance of 10-500 nM EDX in PBS. **B**, Calibration plot of SWV reduction current at −0.8 V (vs. Ag/AgCl) and EDX concentration.

reduction current at −0.8 V (vs. Ag/AgCl) and EDX concentration (Figure 4.4 B) with a R^2 value of 0.9930 and a LOD value of as 23 nM. The LOD of different techniques for EDX determination are summarized in Table 4.1. As could be seen, compared with other techniques and electrodes, BDD electrode could provide more sensitive detection of EDX. These results extremely demonstrate the feasibility of EDX determination on a bare BDD electrode by this method.

Table 4.1 Comparison of LOD obtained through analytical techniques for EDX determination.

Techniques	Linear range	LOD	Reference
HPLC	9.1 μM – 0.36 mM	0.37 μM	[25]
Capillary Electrophoresis	46 μM – 0.23 mM	5.8 μM	[21]
Potentiometry	6 μM – 1 mM	4.2 μM	[20]
SWV, GCE	3.68 μM – 14.7 μM	0.57 μM	[22]
SWV, CPE	1.2 μM – 12 μM	0.26 μM	[26]
SWV, BDD	10 nM – 500 nM	23 nM	This Work

HPLC: High-performance liquid chromatography; SWV: square wave voltammetry; GCE: glassy carbon electrode; CPE: carbon paste electrode

4.3.2 EDX Detection in Plasma

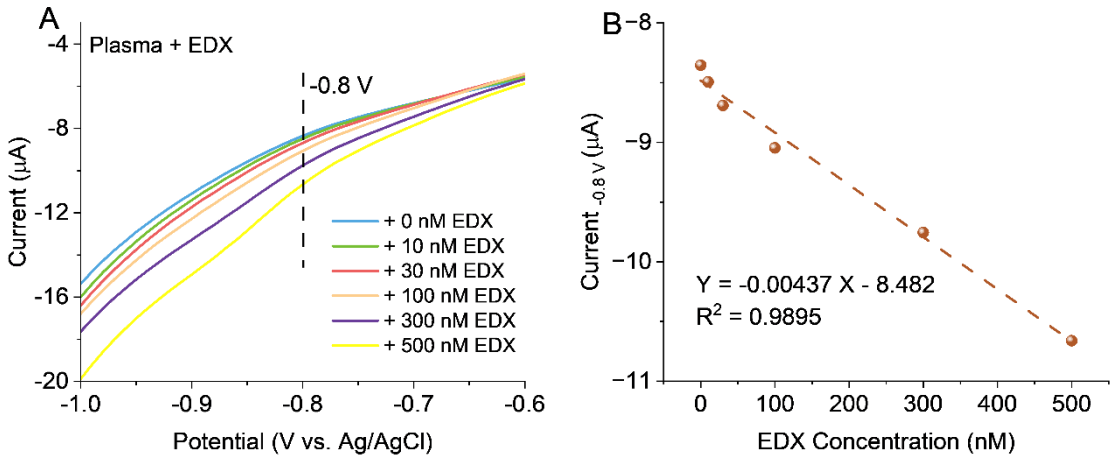

Figure 4.5 EDX detection in human pooled plasma. A, SWV performance of 10-500 nM EDX in plasma. **B**, Calibration plot of SWV reduction current at −0.8 V (vs. Ag/AgCl) and EDX concentration.

A commercial pooled human plasma with 20 donors was used directly after thawing. 10-500 nM EDX was added to the sample and tested by the same electrochemical procedure. As shown in Figure 4.5 A, although no characteristic reduction peak appears, the reduction current value of EDX in plasma increases regularly with the addition of EDX. This indicates that even in complex biofluids like human plasma, BDD electrode is sensitive for detection, owing to BDD electrode has good resistance to non-specific adsorption. A calibration curve between the currents at –0.8 V and EDX concentration is shown in Figure 4.5 B. The concentration dependence indicated this method has the feasibility of EDX determination on a bare BDD electrode.

4.4. Conclusion

This work demonstrated a simple and sensitive electrochemical method for the determination of EDX by using a bare and reusable BDD

electrode. The BDD electrode was used directly after fabrication without any modification. EDX was measured in PBS only by a continuous electrochemical redox procedure without other reagents added. The LOD is 23 nM, which is smaller than other electrodes and techniques. The spiked EDX in human plasma were measured by the same procedure, and the concentration dependence indicates this method has the feasibility of EDX determination on bare BDD.This sustainable and low-cost method of plasma EDX measurement could provide reliable and constant monitoring of emergent anticoagulants in clinic and home health management. This simple electrochemical of drug detection could also offer a wide scope of simple and accurate monitoring of other biomarkers in human biofluids.

4.5 Reference

[1] Levine, S. R. Hypercoagulable states and stroke: A selective review. *CNS Spectrums* **2005**, 10, 567-578.

[2] Mruthunjaya, A. K. V.; Torriero, A. A. J. Electrochemical monitoring in anticoagulation therapy. *Molecules* **2024**, 29, 1453.

[3] Fang, J.; Alderman, M. H. Dissociation of hospitalization and mortality trends for myocardial infarction in the united states from 1988 to 1997. *Am. J. Med.* **2002**, 113, 208-214.

[4] Feigin, V. L.; Lawes, C. M.; Bennett, D. A.; et al. Stroke epidemiology: A review of population-based studies of incidence, prevalence, and case-fatality in the late 20th century. *Lancet Neurol.* **2003**, 2, 43-53.

[5] White, R. H. The epidemiology of venous thromboembolism. *Circulation* **2003**, 107, 4-8.

[6] Kent, A. P.; Brueckmann, M.; Fraessdorf, M.; et al. Concomitant oral anticoagulant and nonsteroidal anti-inflammatory drug therapy in patients

with atrial fibrillation. *J. Am. Coll. Cardiol.* **2018**, 72, 255-267.

[7] Otto, C. M. Heartbeat: Warfarin therapy for mechanical heart valves. *Heart* **2017**, 103, 175-176.

[8] Whitlock, R.; Belley-Cote, E. P.; Healey, J.; et al. Vitamin K antagonists versus direct oral anticoagulants after cardiac surgery: A 31-country cohort study. *Eur. Heart J.* **2020**, 41, ehaa946.0655.

[9] Kakkos, S. K.; Gohel, M.; Baekgaard, N.; et al. Editor's choice - European society for vascular surgery (ESVS) 2021 clinical practice guidelines on the management of venous thrombosis. *Eur. J. Vasc. Endovasc. Surg.* **2021**, 61, 9-82.

[10] Pathak, V.; Allender, J. E.; Grant, M. W. Management of anticoagulant and antiplatelet therapy in patients undergoing interventional pulmonary procedures. *Eur. Respir. Rev.* **2017**, 26, 170020.

[11] Heestermans, M.; Poenou, G.; Hamzeh-Cognasse, H.; et al. Anticoagulants: A short history, their mechanism of action, pharmacology, and indications. *Cells* **2022**, 11, 3214.

[12] Gomez-Outes, A.; Suarez-Gea, M. L.; Lecumberri, R.; et al. Direct-acting oral anticoagulants: Pharmacology, indications, management, and future perspectives. *Eur. J. Haematol.* **2015**, 95, 389-404.

[13] Ogata, K.; Mendell-Harary, J.; Tachibana, M.; et al. Clinical safety, tolerability, pharmacokinetics, and pharmacodynamics of the novel factor Xa inhibitor edoxaban in healthy volunteers. *J. Clin. Pharmacol.* **2010**, 50, 743-753.

[14] Cuker, A.; Husseinzadeh, H. Laboratory measurement of the anticoagulant activity of edoxaban: A systematic review. *J. Thromb. Thrombolysis* **2015**, 39, 288-294.

[15] Gosselin, R. C.; Adcock, D. M.; Bates, S. M.; et al. International Council for Standardization in Haematology (ICSH) recommendations

for laboratory measurement of direct oral anticoagulants. *Thromb. Haemost.* **2018**, 118, 437-450.

[16] Ruff, C. T.; Giugliano, R. P.; Braunwald, E.; et al. Association between edoxaban dose, concentration, anti-factor Xa activity, and outcomes: An analysis of data from the randomised, double-blind ENGAGE AF-TIMI 48 trial. *Lancet* **2015**, 385, 2288-2295.

[17] Younis, S. E.; El-Nahass, S. A.; Elkhatib, M. A. W.; et al. Gradient HPLC-dad method for quantification of novel oral anticoagulant "edoxaban" in plasma: Its selective determination in presence of sixteen co-administered drugs. *J. Chromatogr. B* **2020**, 1160, 122386.

[18] Gouveia, F.; Bicker, J.; Santos, J.; et al. Development, validation and application of a new HPLC-dad method for simultaneous quantification of apixaban, dabigatran, edoxaban and rivaroxaban in human plasma. *J. Pharm. Biomed. Anal.* **2020**, 181, 113109.

[19] Hanada, K.; Matsumoto, S. I.; Shibata, S.; et al. A quantitative LC/MSMS method for determination of edoxaban, a Xa inhibitor and its pharmacokinetic application in patients after total knee arthroplasty. *Biomed. Chromatogr.* **2018**, 32, e4213.

[20] Ayish, N. S.; Marzouk, H. M.; El-Zeany, B. A.; et al. A novel nanoparticles-based electrochemical sensing platform for sensitive detection of oral anticoagulant; edoxaban in human plasma. *Electroanalysis* **2022**, 34, 1266-1272.

[21] Oliveira Rocha, M.; Bordignon Primieri, G.; Ribeiro Wingert, N.; et al. Development and validation of capillary zone electrophoresis and high-performance liquid chromatography methods for the determination of oral anticoagulant edoxaban in pharmaceutical tablets. *Electrophoresis* **2022**, 43, 1617-1625.

[22] Kilic, A.; Aslan, M.; Levent, A. Investigation of the electrochemical properties of edoxaban using glassy carbon and boron-doped diamond

electrodes and development of an eco-friendly and cost effective voltammetric method for its determination. *Anal. Biochem.* **2024**, 685, 115386.

[23] Ishii, K.; Ogata, G.; Einaga, Y. Electrochemical detection of triamterene in human urine using boron-doped diamond electrodes. *Biosens. Bioelectron.* **2022**, 217, 114666.

[24] Moriyama, H.; Ogata, G.; Nashimoto, H.; et al. A rapid and simple electrochemical detection of the free drug concentration in human serum using boron-doped diamond electrodes. *Analyst* **2022**, 147, 4442-4449.

[25] Reddy, P. S.; Jagarlapudi, V. S. K.; Sekaran, C. B. Determination of edoxaban in bulk and in tablet dosage form by stability indicating high-performance liquid chromatography. *Pharm. Sci.* **2016**, 22, 35-41.

[26] Rocha, M. O.; Dallegrave, A.; Klein, T. M.; et al. Electrochemical oxidation of edoxaban and its determination in pharmaceutical samples and human serum. *Microchem. J.* **2024**, 204, 110926.

Chapter 5 Summary and Future Perspective

5.1 Summary

This thesis aims to develop sustainable biosensing techniques using the electrochemical redox method for simple measurement of metabolites and drugs, decrease the complex modification, and reuse the electrode. In particular, based on boron-doped diamond (BDD) with excellent sensitivity, durability, and resistance to non-specific adsorption, target-selective determination methods have been developed.

In Chapter 2, the study of urinary $NaNO_2$ selective determination is performed without adding any other species, such as enzymes, and using a simple electrochemical approach with an oxidation step followed by reduction. In this work, we focus on the reduction potential range for the measurement, which is different from many previous literature reports on the oxidation reaction. The determination of added sodium nitrite based on cyclic voltammetry or differential pulse voltammetry is employed for two pooled and three individual urine samples. From this, the linear response ranges for sodium nitrite detection are 0.5−10 mg/L and 10−400 mg/L. The results from these urine samples convert well to the calibration curve, with the LOD being clinically relevant.

In Chapter 3, with a similar strategy, urinary creatinine (CRE) was determined on a bare BDD electrode. This measurement consists of continuous electrochemical oxidation and reduction of CRE with added reagents of Cl^- and $NaNO_2$. CRE in the range of 100−2500 mg/L and 5−25 mg/L were detected by a similar method with added $NaNO_2$ into D-PBS. This approach detected two pooled and six individual urine samples diluted with D-PBS and added 30 mg/L $NaNO_2$. The calculated CRE results have good agreement with that obtained from the Jaffé method. This strategy may potentially detect urinary creatinine, which might be clinically valuable.

In Chapter 4, by using a similar oxidation followed by a reduction strategy, edoxaban (EDX) was determined without other reagents on a bare BDD electrode. The study discussed the different electrochemical redox states of EDX on the BDD electrode. The reduction peak for the determination of EDX can be observed only after the electrochemical oxidation process. In PBS, EDX showed a good linearity with LOD smaller than other electrodes and techniques. This indicates the BDD electrode could provide more sensitive detection. EDX in human plasma was measured by the same procedure, the concentration dependence indicates this method has the feasibility of EDX determination on bare BDD.

5.2 Future Perspective

The excellent properties of BDD have been widely explored for wide application. In this thesis, we successfully developed a simple oxidation followed by a reduction procedure by using a BDD electrode for metabolites and drug sensors. Certain non-electroactive chemicals could also be detected indirectly. This thesis takes advantage of BDD characteristics of providing a wide potential window, low background current, and good resistance for non-specific adsorption, targets in complex biofluids, such as human urine and plasma could also be selectively detected.

5.2.1 Machine Learning Prediction

Artificial intelligence (AI) has been successfully applied in many fields such as disease classification and diagnosis, treatment recommendation, and drug dosage determination. Physicians can use AI methods to analyze, model, and understand complex clinical data across a

variety of medical practice areas. The application of this technology in clinical testing and POCT offers unprecedented opportunities to expand access to high-quality healthcare. It is worth noting that high-quality data sets can provide enough training materials for the model to help the model better understand and learn features, thus improving the training quality and prediction accuracy of the model. Realizing this potential will require addressing several challenges, including the wider availability of mobile telecommunications devices connected to accurate data sources and sensors.

5.2.2 Sensing on Bare BDD

Under limited conditions, bare BDD can provide sensitive and stable measurements. Compared with other electrodes, BDD has good anti-nonspecific adsorption properties and is suitable for the measurement of sweat, saliva, urine, plasma, serum, and other complex substrates and biological fluids or high-concentration targets. In addition, for some non-electroactive targets, BDD electrodes with wider potential windows and lower background current can also be used to directly or indirectly measure targets. There is also a need for a clearer understanding of the detection mechanism. In addition to sufficient experimental validation, theoretical studies such as the modeling process of density functional theory (DFT) would be an effective method of theoretical interpretation.

5.2.3 Point-of-care Devices

While laboratory-level experiments and designs can work well to measure targets, small, wearable, or portable instruments are more likely to be preferred in practical applications. In addition, due to the use of untrained or unsupervised personnel, the simplified use process,

especially in pre-analysis (patient preparation, sample collection, identification of invalid samples) and post-analysis (documentation, data protection), is also an area of concern. Especially in areas far from laboratories, such as developing countries and economically underdeveloped areas, POCT analysis is clear and concise, which can meet medical requirements, and also has an important role in laboratory medicine and even overall health management in the future.

List of Publications and Conferences

Published papers presented in this thesis:

(1) ZHANG, Z., Ogata, G., Asai, K., Yamamoto, T., Einaga, Y. "Electrochemical Diagnosis of Urinary Tract Infection Using Boron-Doped Diamond Electrodes",
ACS Sensors, **2023**, 8, 11, 4245 – 4252.
Selected Supplementary Journal Cover

(2) ZHANG, Z., Ogata, G., Einaga, Y.,
"Indirect Electrochemical Detection of Creatinine in Human Urine Samples Using a Bare Boron-Doped Diamond Electrode",
Bulletin of the Chemical Society of Japan, **2025**, 98, 7, uoaf069.

Patent:

(1) 張子平、緒方元気、村田道生、栄長泰明、浅井開

亜硝酸塩の測定方法および亜硝酸塩の測定装置

出願番号: 2023-081350

出願日:2023/5/17

International Conference:

(1) ZHANG, Z., Ogata, G., Asai, K., Yamamoto, T., Einaga, Y.

"Electrochemical Detection of $NaNO_2$ in Human Urine Using Boron-Doped Diamond Electrode",

The Nineteenth International Symposium on Electroanalytical Chemistry (19th ISEAC), August 19th, 2023, Changchun, China

(Excellent Poster Award was got, from top 20 of 175 presenters)

(2) ZHANG, Z., Ogata, G., Einaga, Y.,

"An Indirect Electrochemical Detection Of Creatinine In Urine Samples Using A Boron-Doped Diamond Electrode"

NanoBalkan 2024, October 31th, 2024, Tirana, Albania

Domestic Conference:

(1) ZHANG, Z., Ogata, G., Asai, K., Yamamoto, T., Einaga, Y.

"Electrochemical Detection of $NaNO_2$ in Human Urine Using Boron-Doped Diamond Electrode",

The Electrochemical Society of Japan (ECSJ) Fall Meeting 2023, September 11th, 2023, Kyushu, Japan

Acknowledgment

This PhD thesis is finished in the memorable year of 2025. There is an old saying in Chinese called a person forms his opinion and judgment at the age of thirty. I am 30 years old and going to obtain the highest degree of my life. Looking back on the past, everything is so memorable.

I enrolled PhD program at Keio University in 2021. Unfortunately, due to the COVID-19 pandemic sweeping the world, I could not obtain a visa to Japan in time and the flights were suspended that year. Unexpectedly, I stayed in China for one year and entered Japan in April 2022. This is my first country to go abroad. Before I came here, all I knew about it was records in history books and TV shows. With the idea of “Come and see by myself” in mind, I started my study abroad trip.

Here, I meet my supervisor, Prof. Einaga and Ogata Sensei. I sincerely express my deep gratitude to them. During my time at Keio University, my research was not so smooth. Since the master's research direction is photocatalysis, I always made slower progress here than other students at the beginning. I often got “bad data”, making me anxious and frustrated. However, they always tell me that there is no useless data, and there is always valid information behind every data. Slowly, I came to realize that this is indeed the case. Although not all the data can be included in the article, it can deepen our understanding of the research. This has greatly changed my perception of research. I had always assumed that successful researchers would always be able to quickly find the key points in a lot of complex phenomena, and I had overlooked this kind of experience or scientific intuition that needs to be accumulated over time. After that, I gradually learned to enjoy the process of research,

which I think is one of the biggest achievements of my PhD.

In addition, I would like to thank all the reviewers of my doctoral defense, Prof. Daniel Citterio, Prof. Taku Hasobe, and Prof. Teruhiko Matsubara for all the kind suggestions and comments for my work. I am also grateful for the revision of this graduation thesis, which makes it better than before.

Additionally, I sincerely thank all the members of the Einaga lab, both staff and students, for their kind help and companionship in academic study and life. This enables me to successfully go through the difficult period at the beginning and quickly enter the state of study and life.

Besides, I also want to thank my family. Thanks for the unwavering support for my studying abroad. The support I've had has kept me going.

Lastly, I would like to send my best gratitude to the Japan Student Service Organization (JASSO), Goldman Sachs Scholars Fund, Keio University, and JGC-S Scholarship Foundation for the scholarship for international students. With the support of these scholarships, I could concentrate more on my research and life in Japan.

I hope that the work done in this thesis will help advance science and technology, especially in the field of electrochemical sensors for POCT.

Japan,

September 2025

Zhang